

Detrital zircon U–Pb–Hf systematics of Ediacaran metasediments from the French Massif Central: Consequences for the crustal evolution of the north Gondwana margin

Simon Couzinié, Oscar Laurent, Cyril Chelle-Michou, Pierre Bouilhol, Jean-Louis Paquette, Abdelmouhcine Gannoun, Jean-François Moyen

▶ **To cite this version:**

Simon Couzinié, Oscar Laurent, Cyril Chelle-Michou, Pierre Bouilhol, Jean-Louis Paquette, et al.. Detrital zircon U–Pb–Hf systematics of Ediacaran metasediments from the French Massif Central: Consequences for the crustal evolution of the north Gondwana margin. Precambrian Research, 2019, 324, pp.269-284. 10.1016/j.precamres.2019.01.016 . hal-02026217

HAL Id: hal-02026217
https://uca.hal.science/hal-02026217

Submitted on 22 Oct 2021

HAL is a multi-disciplinary open access archive for the deposit and dissemination of scientific research documents, whether they are published or not. The documents may come from teaching and research institutions in France or abroad, or from public or private research centers.

L'archive ouverte pluridisciplinaire **HAL**, est destinée au dépôt et à la diffusion de documents scientifiques de niveau recherche, publiés ou non, émanant des établissements d'enseignement et de recherche français ou étrangers, des laboratoires publics ou privés.



Distributed under a Creative Commons Attribution - NonCommercial| 4.0 International License

Version of Record: https://www.sciencedirect.com/science/article/pii/S0301926818304017
Manuscript_fcf4e64cf64712b7f94281eaaf045b4b

Detrital zircon U–Pb–Hf systematics of Ediacaran metasediments from the French Massif Central: consequences for the crustal evolution of the north Gondwana margin

Simon Couzinié[1,2,3*], Oscar Laurent[4], Cyril Chelle-Michou[4,5], Pierre Bouilhol[3], Jean-Louis Paquette[6], Abdel-Mouhcine Gannoun[6], Jean-François Moyen[2]

[1]Université de Lyon, ENSL, UCBL, CNRS, LGL-TPE, F-69007 Lyon, France

[2]Université de Lyon, Laboratoire Magmas et Volcans, UJM-UCA-CNRS-IRD, F-42023 Saint-Étienne, France

[3]CRPG, Université de Lorraine, CNRS, UMR7358, 15 rue Notre Dame des Pauvres, F-54501 Vandoeuvre Les Nancy, France.

[4]Institute for Geochemistry and Petrology, ETH Zürich, Zurich, Switzerland

[5]School of Earth Sciences, University of Bristol, Wills Memorial Building, Queens Road, Bristol BS8 1RJ, UK

[6]Université Clermont Auvergne, CNRS, IRD, OPGC, Laboratoire Magmas et Volcans, F-63000 Clermont-Ferrand, France

*corresponding author. simon.couzinie@univ-lorraine.fr

Abstract 2
1. Introduction 3
2. Geological setting 6
3. Samples and analytical techniques 7
4. Results 9
4.1 Zircon description 9
4.2 U–Pb geochronology 10
4.3 Zircon Hf isotope compositions 11
5. Discussion 13

© 2019. This manuscript version is made available under the Elsevier user license
http://www.elsevier.com/open-access/userlicense/1.0/
© 2019 published by Elsevier. This manuscript is made available under the CC BY NC user license
https://creativecommons.org/licenses/by-nc/4.0/

5.1 Interpretation of U–Pb dates: depositional ages of the sedimentary protoliths and Variscan overprint 13
5.2 The Ediacaran paleogeography of the EFMC with respect to other Variscan zones 15
5.3 Zircon sources 17
5.4 Crustal evolution of the EFMC and the North Gondwana margin 22
6. Conclusion 24
Acknowledgements 26
Figures captions 26
References 29

Abstract

Combining U–Pb and Lu-Hf isotopic data of detrital zircon grains has proven a powerful tool to unravel the provenance of sediments and address continental crust evolution. In this study, we explore the origin of thick siliciclastic metasedimentary units from the high-grade internal domains of the Variscan belt of Europe and examine their significance for Neoproterozoic crust formation and evolution along the North Gondwana margin. We present data and U–Pb/Lu–Hf systematics of detrital zircons from five amphibolite-facies metasediments sampled in the eastern French Massif Central, measured in situ by LA–(MC)–ICP–MS. The sedimentary protoliths were deposited in the Ediacaran as evidenced by field relationships and maximum depositional ages ranging between 592.4 ± 5.5 and 556.8 ± 5.1 Ma. All samples contain three main zircon populations in terms of age distribution and Hf isotopes: (i) abundant 0.55–0.65 Ga zircons with considerably scattered $\varepsilon Hf_{(t)}$ from -19 to +14; (ii) varied amounts of 0.65–1.0 Ga zircons showing dominantly positive $\varepsilon Hf_{(t)}$ with the exception of the c. 1.0 Ga zircons; and (iii) ≥ 1.8 Ga zircons (mostly between 1.9–2.1 and 2.5–2.8, up to 3.2 Ga) with $\varepsilon Hf_{(t)}$ ranging between +5 and -7. Multidimensional scaling of our U–Pb dataset and a data compilation of Ediacaran to Lower Cambrian

(meta)sediments from the North Gondwana margin reveals that the relative proportions of the three age components carry discriminant provenance information. Geological data indicate that the Ediacaran basins of the eastern French Massif Central collected the erosion products of two main source regions: (i) the Neoproterozoic Cadomian magmatic arc; and (ii) the cratonic hinterland, mostly from the Saharan Metacraton and the Arabian-Nubian Shield. Our dataset attests to the reworking of: (i) juvenile Neoproterozoic crust and, (ii) old Paleoproterozoic to Neoarchean crustal components, either as part of the detritus or incorporated in Neoproterozoic arc magmas. First-order estimates derived from the isotopic signature of S-type granitic magmas sourced in the Ediacaran metasediments suggest that 60–75% of the detritus would correspond to young Neoproterozoic crust and thus represent net additions to the continental crust volume.

Keywords: North Gondwana margin, French Massif Central, detrital zircons, U–Pb–Hf isotopes, Cadomian orogeny, crustal growth

1. Introduction

Multi-methods studies based on surface heat flow measurements, seismic profiles and large-scale geochemical surveys concluded that the continental crust has a bulk andesite/diorite composition (e.g. Rudnick and Fountain (1995); Rudnick and Gao (2003); Wedepohl (1995)). Importantly, such composition is not in equilibrium with a mantle peridotite, meaning that new crust generation necessitates the addition of mantle-derived magmas to a pre-existing crustal volume followed by differentiation of the basaltic precursor and foundering of mafic residual materials into the mantle. This hints that the hallmark of crust production is the intrusion of magmas extracted from

ultrabasic and young basic igneous sources (Condie and Aster, 2010). However, addressing the rate of crust production based solely on the igneous record has proven ambiguous because magmatic rocks are not always preserved and can experience sedimentary reworking (Iizuka et al., 2005). Consequently, continental sediments and sedimentary rocks have been increasingly used to address the timing, rate and mode of continental crust formation (see review in Dhuime et al. (2017)). In particular, many studies focus on zircon, an accessory mineral of intermediate to felsic igneous rocks characterized by its extreme resilience to mechanical abrasion and low to high-T alteration such that it is very commonly retrieved as detrital grains in sedimentary lithologies. Chronological constraints derived from detrital zircon U–Pb systematics paired with the determination of Lu–Hf isotope compositions of individual grains offer the possibility to gain insights on the age and origin of rocks that have been eroded and thus to genuinely track periods of crust production (Gerdes and Zeh, 2006; Iizuka et al., 2005; Kemp et al., 2006).

The basement of Western and Central Europe corresponds to a set of crustal blocks amalgamated during the late Paleozoic Variscan *s.l.* collisional orogeny (Franke, 1989; Kroner and Romer, 2013; Matte, 1986). Such blocks are often referred to as 'Cadomian-type peri-Gondwana terranes' since they were formerly located at the northern margin of the Gondwana continent by the late Neoproterozoic and were strongly shaped by the Cadomian accretionary orogen featuring a c. 2500 km-long magmatic arc and associated back-arc basin (Garfunkel, 2015; Murphy and Nance, 1989; Murphy et al., 2004). Importantly, accretionary orogenic settings are generally retained as the main sites of continental crust production as they encompass voluminous mantle-derived magmatism (Cawood et al., 2009; Reymer and Schubert, 1984; Taylor and McLennan, 1985). Yet, within the Cadomian realm, today-exposed mantle-derived volcanic-plutonic associations are scarce, in marked contrast with the

well-preserved coeval siliciclastic sedimentary successions deposited at the rear of the arc (Dabard et al., 1996; Denis and Dabard, 1988; Drost et al., 2011; Garfunkel, 2015; Linnemann et al., 2014; Linnemann et al., 2008; Orejana et al., 2015; Pereira et al., 2006; Pereira, 2014; Pereira et al., 2012a; Pereira et al., 2012b; Rabu et al., 1990; Talavera et al., 2015; Talavera et al., 2012). Therefore, such sedimentary rocks would have preserved the best record of the Cadomian orogenic evolution and constitute an ideal target to clarify the extent of Neoproterozoic crust production along the North Gondwana margin.

Several provenance studies based on heavy minerals or detrital zircon typology and U–Pb(–Hf) signatures have been carried out with the main aim to address the Neoproterozoic paleogeography of the peri-Gondwana terranes, notably their paleo-location along the main Gondwana continent (e.g., (Chelle-Michou et al., 2017; Dabard et al., 1996; Drost et al., 2011; Henderson et al., 2016; Pereira et al., 2012a; Pereira et al., 2012b; Stephan et al., 2018). Investigations so far focused on areas having experienced limited Variscan metamorphic overprint such as the Teplá-Barrandian and Saxo-Thuringian zones of the Bohemian Massif (Drost et al., 2011; Hajná et al., 2017; Linnemann et al., 2007; Linnemann et al., 2014; Linnemann et al., 2017; Žák and Sláma, 2017), the Central Iberian, Ossa-Morena and Cantabrian zones of the Iberian Massif (Díez Fernández et al., 2010; Fernández-Suárez et al., 2014; Naidoo et al., 2017; Orejana et al., 2015; Pereira et al., 2012a; Pereira et al., 2012b; Talavera et al., 2015; Talavera et al., 2012; Teixeira et al., 2011; Zimmermann et al., 2015) and the northern to central Armorican Massif (Ballouard, 2016; Dabard et al., 1996; Denis and Dabard, 1988; Gougeon et al., 2017; Nagy et al., 2002; Rabu et al., 1990), all exposing (very) low to medium-grade Variscan metamorphic units (Fig. **1**). In contrast, little is known about the pre-orogenic evolution of the high-grade metamorphic belts building up the Moldanubian zone, regarded as the most internal domain of the Variscan belt

(Lardeaux et al., 2014). In this contribution, we report the U–Pb–Hf isotopic compositions of detrital zircon grains from amphibolite-facies metasediments from the eastern French Massif Central measured in situ by LA–(MC)–ICP–MS with the aim to address: (i) the Neoproterozoic paleogeography of this crust segment with respect to adjacent (para)autochtonous Variscan blocks; (ii) the source of the sedimentary supplies; (iii) the relative extent of crust production/reworking during the Cadomian orogeny.

2. Geological setting

The eastern French Massif Central (EFMC, Fig. **2**) exposes two main allochtonous tectonic-metamorphic units (nappes), juxtaposed as a result of collision between Laurussia and Gondwana (Faure et al., 2009b; Ledru et al., 1989). The overlying *Upper Gneiss Unit* comprises ortho- and paragneisses having experienced MP–M(H)T amphibolite- to granulite-facies collisional metamorphism at 360–340 Ma (Chelle-Michou et al., 2017). The base of this unit features a bimodal meta-igneous association referred to as the Leptynite-Amphibolite Complex, which hosts petrological relicts of eclogite-facies metamorphism dated at c. 380 Ma in the SW part of the French Massif Central (Lotout et al., 2018), presumably attesting to the closure by subduction of the Galicia-Massif Central oceanic domain. The underlying Lower Gneiss Unit consists of an association of amphibolite-facies micaschists, ortho- and paragneisses with very scarce amphibolites (Ledru et al., 2001). The *Lower Gneiss Unit* experienced significant anatexis at the post-collisional stage (315–300 Ma, e.g. Mougeot et al. (1997)), culminating in the formation of the 120 x 80 km large Velay granite-migmatite dome during orogenic collapse (Ledru et al., 2001; Montel et al., 1992). The Velay dome is overturned to the south onto the low-grade *Parautochtonous Unit*, largely

composed of greenschist- to lower amphibolite-facies metasediments. All metamorphic units were intruded by a set of peraluminous to metaluminous granitoids, testifying for protracted magmatic activity between 335 and 300 Ma (Couzinié et al., 2014; Laurent et al., 2017; Villaros et al., 2018).

Available geochronological data on the protoliths of the metamorphic rocks from the EFMC suggest contrasted pre-Variscan evolutions for each nappe. In the Upper Gneiss Unit, both felsic and mafic meta-igneous lithologies are of Ordovician age (LA–ICP–MS U–Pb and Pb evaporation zircon ages; Chelle-Michou et al. (2017); Feybesse et al. (1995)). Metasediments have not been investigated in the EFMC area but yielded Cambrian maximum depositional ages in the western part of the French Massif Central (LA–ICP–MS U–Pb zircon; Melleton et al. (2010)). In the Lower Gneiss Unit, the protoliths of the Velay Orthogneiss Formation (Fig. **2**), an association of augen gneisses and leucogneisses regarded as former S-type granites, were emplaced at c. 541 Ma (LA–ICP–MS U–Pb zircon; Couzinié et al. (2017)), i.e. at the Ediacaran–Cambrian transition. Field relationships indicate that these (meta)granites are intrusive within the (meta)sediments of the Lower Gneiss Unit (Ledru et al., 1994) entailing that the latter were deposited in the Precambrian. The abundance of Neoproterozoic inherited zircon cores in the Velay Orthogneiss Formation and other crust-derived Variscan granitoids point to a Neoproterozoic crustal source which likely corresponds to the metasediments (Couzinié et al., 2017; Laurent et al., 2017). This view is consistent with the preliminary results of Chelle-Michou et al. (2017) who obtained 25 concordant Neoproterozoic U–Pb zircon dates from a Lower Gneiss Unit paragneiss. Finally, deposition of the thick siliciclastic successions of the Parautochtonous Unit was bracketed by LA–ICP–MS U–Pb zircon dating of interlayered felsic volcanics, all yielding Ordovician ages (Faure et al., 2009a).

3. Samples and analytical techniques

The sampling strategy was to cover all the metasedimentary units wrapping the Velay migmatite-granite dome, which cores the Lower Gneiss Unit in the EFMC. Five amphibolite-facies metasediments were collected. GPS coordinates and whole-rock major and trace element compositions of the investigated samples are available in Supplementary Table S1. The latter were obtained from the ALS Global firm (details on the procedure and accuracy/reproducibility in Supplementary Material).

PIL-16-01 belongs to a 40 cm-thick metasandstone body interbedded within the aluminous Pilat micaschists (Malavielle et al., 1990), which form a constituent lithology of the Lower Gneiss Unit in the northern part of the Velay Complex (Fig. **2**). This very silicic rock (SiO_2 > 87%) is dominantly composed of quartz and muscovite with subordinate amounts of feldspar, Fe–Ti oxides and zircon (Fig. **S1a**). The metamorphic evolution has been constrained on surrounding metapelites and features an early stage at 8–10 kbar and 600 ± 50°C followed by equilibration at 3–5 kbar and 690 ± 20°C (Gardien, 1990).

SEN-16-01 corresponds to a meter-thick quartz-rich layer within the Senouire micaschists, a typical metasedimentary unit of the western flank of the Velay Complex (Ledru et al., 1994). The specimen is mostly composed of quartz and biotite with minor amounts of muscovite, garnet, plagioclase, Fe–Ti oxides and zircon (Fig. **S1b**). Peak metamorphic conditions for this unit have been estimated at 630 ± 20°C and 5–6 kbar (Mintrone, 2016).

CHA-16-02 was sampled from a 20 cm-thick meta-arkose layer closely associated with amphibolite-facies micaschists from the southwestern part of the Velay Complex (Briand et al., 1993). The rock is clearly a meta-arkose because of its moderate SiO_2/Al_2O_3 and Fe_2O_3/K_2O ratios (lower than 6 and 0.7 respectively; Herron (1988)) and

the high modal proportion of feldspar which, together with quartz, constitutes most of the rock. Other minerals include garnet, muscovite, Fe–Ti oxides and zircon (Fig. **S1c**). *TN46* is a coarse-grained, anatectic paragneiss collected in the eastern part of the dome in the Tournon area (Fig. **2**) and already described in Chelle-Michou et al. (2017). The sample is dominantly composed of quartz, plagioclase, alkali-feldspar and biotite together with scarce sillimanite.

PdB-16-01 is an anatectic paragneiss taken from the migmatite exposure of Pont de-Bayzan in the southern part of the dome (described in Montel et al. (1992)). Only the melanocratic part of the sample, presumably corresponding to residuum in the sense of Sawyer (2008), was selected for zircon analysis. The mineral assemblage consists of quartz, plagioclase, alkali-feldspar and biotite with accessory zircon, monazite and apatite (Fig. **S1d**). According to Montel et al. (1992), partial melting took place at 650–720°C and 3–4.5 kbar.

Zircon grains were separated from crushed rock samples using standard techniques at Saint-Etienne University, described in Couzinié et al. (2016). More than 100 and up to 300 randomly selected grains were cast in epoxy resin and polished down to an equatorial grain section. Cathodoluminescence imaging was performed at (i) the Laboratoire Magmas et Volcans in Clermont-Ferrand, France using a Jeol JSM-5910 and (ii) the University of Bristol, UK using a Hitachi S-3500N SEM. Zircon U–Pb isotopic analyses were carried out at ETH Zürich, Switzerland by laser ablation–inductively coupled plasma–sector field–mass spectrometry (LA–ICP–SF–MS) using a RESOlution (ASI, Australia) 193 nm ArF excimer laser system coupled to an Element XR (Thermo Scientific, Germany) sector-field mass spectrometer. Lu-Hf isotope measurements were performed at the Laboratoire Magmas et Volcans using a Thermo Scientific Neptune Plus multi-collector ICP–MS coupled to the same RESOlution 193 nm laser excimer system as described above. Comprehensive descriptions of the

methodologies, results of secondary standard and sample measurements for both U-Pb and Lu-Hf isotopes are available as Supplementary Material and Supplementary Table S2 to S5.

4. Results

4.1 Zircon description

Zircon grains in the investigated samples are mostly colorless, a few of them being pinkish or yellowish. Their shapes vary from rounded (notably in sample PIL-16-01) to sub-idiomorphic (sample PdB-16-01) with aspect ratios up to 1:3. They range in length from 50 to 160 µm except in sample TN46 from which markedly larger grains were extracted (100 to 300 µm long). The zircon grains are often broken (particularly in samples PIL-16-01 and SEN-16-01). Cathodoluminescence images reveal very diverse internal structures (Fig. **3**). Oscillatory or patchy, broad zoning is common in many grains (see for instance in PdB-16-01, Fig. **3e**). Core-rim relationships are frequent in sample TN46 (e.g. z19, z54 and z84 in Fig. **3d**) but generally lacking in other samples in which only very few crystals show narrow CL-bright or dark rims (< 10 µm-wide, see zircon z83 and z35, Fig. **3a**, or z11, Fig. **3b**). Secondary textures include healed cracks and fractures (e.g. z35, Fig. **3a**) and zones of blurred oscillatory zoning (e.g. z146, Fig. **3c**), which were avoided for U-Pb dating. Otherwise, we did not target any specific population in an attempt to be representative of the overall zircon diversity.

4.2 U–Pb geochronology

A total of 745 U–Pb measurements were performed on zircon grains from the five metasediments. Only dates concordant at 95–105% (with concordance defined as $^{206}Pb/^{238}U$ date / $^{207}Pb/^{206}Pb$ date x 100) will be further considered for interpretation (representing 492 individual analyses). The $^{206}Pb/^{238}U$ dates are reported when younger than 1.2 Ga; the $^{207}Pb/^{206}Pb$ dates are preferred when older. The preliminary zircon U–Pb–Hf data obtained by Chelle-Michou et al. (2017) on sample TN46 were appended to our new dataset of 67 U–Pb analyses on this sample.

The detrital zircon date distributions of all samples feature a dominant Ediacaran to late Cryogenian population in the range 550–720 Ma representing between 50 and 75% of the dates and defining a prominent peak at c. 635 Ma (Fig. **4, 5**). The remaining analyses are mostly distributed over three main periods: 760–1050 Ma (Tonian to late Stenian), 1.7–2.1 Ga (Paleoproterozoic) and 2.6–3.2 Ga (Neo- to Paleoarchean). PIL-16-01 and CHA-16-02 show similar detrital zircon date distributions, with the Ediacaran–Cryogenian and Tonian–Stenian populations representing c. 70% and 14% of the dataset, respectively (Fig. **4a,c** and **5a,c**). Paleoproterozoic and Archean dates are relatively scarce (< 12% and 6%, respectively). Sample SEN-16-01 differs by a larger proportion of 760–1050 Ma and older-than-1.8 Ga grains (18 and 23%, respectively, Fig. **5b**). TN46 paragneiss contains very few Tonian–Stenian grains but an abundant Paleoproterozoic-Neoarchean population (36%, Fig. **5d**), with dates up to 3.27 Ga (spot z7). The zircon U–Pb date spectrum of PdB-16-01 contrasts with that of the other samples because: (i) Tonian–Stenian grains are more abundant than in any other sample, representing 38% of the dataset; and (ii) Paleoproterozoic and Neoarchean dates are very scarce (only 4% of the data) (Fig. **5e**). CL-dark zircon grains yielding Variscan dates in the range 320–305 Ma were retrieved in sample TN46, as already described and discussed by Chelle-Michou et al. (2017).

4.3 Zircon Hf isotope compositions

The zircon grains analyzed for Lu–Hf isotopes were selected as to representatively capture the zircon date distribution for each sample. The results are depicted Fig. **6**.

PIL-16-01. Twenty-two 550–665 Ma zircon grains show very diverse εHf(t), from +8.7 down to -10.5. One late Tonian grain has a radiogenic εHf(t) of +4.6. Early Tonian to late Stenian zircons also have variable Hf isotope signatures with 3 grains displaying εHf(t) of -11.9, +1.6 and +10.8 ε-units. Five Paleoproterozoic zircons range between -7.4 and +4.0 ε-units. Three Neoarchean grains are chondritic to suprachondritic, with εHf(t) ranging from -0.4 up to +4.1.

CHA-16-02. The Hf isotope signature of 32 Ediacaran–Cryogenian zircons (565–720 Ma) is highly scattered with εHf(t) ranging from -16.9 up to +12.7. Tonian–Stenian (n=6) and Paleoproterozoic (n=1) grains display chondritic to supra-chondritic εHf(t) (between +0.5 and +12.3). Three Neoarchean zircons are nearly chondritic with εHf(t) ranging between -2.0 and +1.2.

PdB-16-01. Zircons with U–Pb dates in the range 590–980 Ma have dominantly very radiogenic Hf isotope signatures: 84% of the data yield εHf(t) higher than +4.4, and 47% show values overlapping with those for the Depleted Mantle (up to +13.7). Beside this, 8% are nearly chondritic (between -1.8 and 1.2) and the remaining 8% subchondritic (between -12.1 and -18.7). Paleoproterozoic zircon grains show slightly non-radiogenic signatures (εHf(t) of c. -2). Two Neoarchean grains yielded sub and suprachondritic values of -5.6 and +2.6.

TN46. Results for this sample were obtained by Chelle-Michou et al. (2017) and are briefly summarized hereafter. Zircon grains with U–Pb dates in the range 560–650 Ma show very scattered εHf(t) ranging from +5.6 down to -19.1. Two early Cryogenian–Tonian grains have identical and very radiogenic Hf isotope signatures of +7.5. Four Paleoproterozoic grains display unradiogenic signatures with εHf(t) between -3.0 and -15.5. Archean zircons have chondritic to negative εHf(t) between +0.2 and -4.2.

General pattern. The εHf(t) measured on Paleoproterozoic and Archean zircon are highly scattered from sub to suprachondritic values. Detrital zircons crystallized at the Tonian–Stenian boundary have even more diverse signatures with εHf(t) ranging from -19 up to +11 (in the field of composition expected for the Depleted Mantle reservoir). A large majority of early Cryogenian–Tonian zircons (mostly represented by sample Pdb-16-01) have very radiogenic Hf isotope signatures. Ediacaran–late Cryogenian zircon grains are typified by their highly variable εHf(t), from -19.1 up to +12.2.

5. Discussion

5.1 Interpretation of U–Pb dates: depositional ages of the sedimentary protoliths and Variscan overprint

Field relationships indicate that (meta)granites from the Velay Orthogneiss Formation are intrusive within the (meta)sediments of the Lower Gneiss Unit (Ledru et al., 1994). The oldest emplacement age determined for the metagranite samples (545.9 ± 4.3 Ma, leucogneiss MM09; Couzinié et al. (2017)) entails that the minimum depositional age of the sediments is Ediacaran. One single spot (#116) from a zircon grain in sample PIL-16-01 yielded a concordant date that is significantly younger than this inferred minimum

deposition age, i.e. 526 ± 5 Ma (Fig. 5a). This zircon grain is therefore regarded as an outlier, which possibly experienced Pb loss. Excluding this grain, all dates are older than c. 545 Ma, so that the youngest zircon population in each sample can be reasonably considered as representative of the maximum deposition age. The latter has been estimated via the following procedure. First, the youngest (and older than c. 545 Ma) concordant analysis is identified. A Concordia date is then calculated out of it and the closest older analysis. If the MSWD of concordance and equivalence lies in the range of acceptable values (which depends on the number of analyses, see Spencer et al. (2016)), the dates are statistically indistinguishable. The next older analysis is then added to this pool and a new Concordia date calculated. This procedure is repeated until the MSWD falls out of the acceptable range. Maximum depositional ages range from 592.4 ± 5.5 Ma for sample PdB-16-01 down to 556.8 ± 5.1 Ma for PIL-16-01 (Fig. **4**). Samples SEN-16-01, CHA-16-02 and TN46 show intermediate (and identical) maximum depositional ages of 567.7 ± 6.0, 568.3 ± 4.9 and 566.3 ± 6.2 Ma, respectively.

Among the five samples, zircon grains yielding Variscan dates were only retrieved from the anatectic paragneiss TN46 for which a Concordia date of 307.3 ± 5.1 Ma ($MSWD_{C+E}$ = 1.3) can be calculated out of three equivalent analyses. Following Chelle-Michou et al. (2017), we interpret this date as reflecting the age of partial melting in this part of the Lower Gneiss Unit. Apart from this sample, our dataset is indicative of scant zircon neo- and/or re-crystallization during Variscan metamorphism as Variscan grains are commonly lacking and overgrowth zones are scarce and narrow. Even though the investigated samples equilibrated at amphibolite-facies conditions, reaching partial melting for two of them, the Variscan imprint on the zircon budget remained very limited, and the zircon age distribution clearly records the pre-Variscan evolution of the protoliths.

5.2 The Ediacaran paleogeography of the EFMC with respect to other Variscan zones

In this section, we aim to identify the provenance of the crustal segment that constitutes the high-grade Lower Gneiss Unit of the EFMC by addressing its paleographic relationships with adjacent, non-metamorphic to low-grade Variscan zones. For this purpose, we compiled the results of 19 detrital zircon studies conducted on Ediacaran to Lower Cambrian (meta)sediments from several Variscan zones (Fig. **1**) and compared the detrital zircon date distributions to those observed in the EFMC. Comparison was quantified by non-metric multidimensional scaling (MDS) (Borg and Groenen, 2005), a statistical technique recently expanded to the field of provenance studies (Vermeesch, 2013). A total of 54 samples were retained based on the cut-off criterion “at least 51 zircon dates concordant at 95–105%” (with concordance defined as $^{206}Pb/^{238}U$ date / $^{207}Pb/^{206}Pb$ date x 100), which corresponds to the number of grains needed to be certain at 95% that no fraction representing more than 10% of the actual population has been missed (Vermeesch, 2004). Calculations were computed using the open-source R language (Ihaka and Gentleman, 1996) and the package `provenance` (Vermeesch et al., 2016). As the U–Pb data were obtained from several laboratories, with different analytical methods (LA–ICP–MS, SHRIMP) and associated analytical uncertainties, we used the Sircombe-Hazelton L2-norm (Sircombe and Hazelton, 2004) as dissimilarity measure, as recommended by Vermeesch (2018). The resultant MDS “map” is displayed figure **7a**.

Two major parameters control the variability of the U-Pb date distributions in Ediacaran–Lower Cambrian (meta)sediments from the North Gondwana margin:(i) the proportions of ≥1.8 Ga zircons (captured by Dim_1); and (ii) the relative importance of

400 the Ediacaran–late Cryogenian (<0.65 Ga) vs. early Cryogenian-Tonian (0.65-1.0 Ga)
401 zircons in the Neoproterozoic population (Dim_2) (Fig. **7b**). Specifically, the higher the
402 value of Dim_1, the greater the proportions of zircons with Paleoproterozoic and older U–
403 Pb dates. Samples with elevated Dim_2 (such as NE13–1) feature a unimodal Ediacaran
404 date peak, whereas detrital zircon dates from low-Dim_2 samples (e.g. PNC1) are more
405 evenly distributed throughout the Ediacaran–Tonian time interval.
406
407 In the Dim1-Dim2 projection, Ediacaran–Lower Cambrian (meta)sediments from each
408 Variscan zone plot within restricted domains (Fig. **7a**). Importantly, samples from the
409 Lower Gneiss Unit of the EFMC display a large variety of detrital zircon date
410 distributions among this North Gondwana scheme. Paragneiss sample TN46 contains
411 little 0.65–1.0 Ga zircon but a significant proportion of older-than-1.8 Ga grains, a
412 pattern similar to those observed in Ediacaran–Lower Cambrian (meta)sediments from
413 the Bohemian Massif. In contrast, samples PdB16-01 and SEN16-01 are akin to
414 (meta)sediments of the Central Iberian Zone, being particularly characterized by the
415 abundance of 0.65-1.0 Ga zircons. PIL16-01 and CHA16-01 plot in an intermediate
416 position with respect to these two endmembers. Altogether, the samples from the
417 EFMC Lower Gneiss Unit straddle the fields outlined by all the other Variscan zones
418 and no perfect match exists with any of them. Consequently, if the EFMC
419 metasediments were originally part of a single sedimentary basin (as suggested by
420 geological evidence), such basin can be regarded as a singular Ediacaran
421 paleogeographic domain. The marked variations of the detrital zircon date distributions
422 between individual samples of the EFMC can be interpreted in two different ways. A
423 first possibility would be to consider that they reflect lateral and local variations of the
424 sediment supply within the Ediacaran basin. Alternatively, they could indicate an
425 evolution of the sources of the detritus throughout the Ediacaran (of which timescales
426 cannot be captured within the precision of the LA-ICP-MS dating and the lack of

427 stratigraphic relationship between the samples), i.e. changes in paleo-streams and/or
428 tectonic setting delivering eroded materials from at least two different areas.
429
430 ## 5.3 Zircon sources
431
432 Multi-methods studies (encompassing geochemistry, petrography, sedimentology,
433 geochronology) have demonstrated that Ediacaran sediments deposited along the
434 northern margin of Gondwana were of mixed origin. A fraction of the detritus originated
435 from the erosion of the Cadomian magmatic arc and the rest was supplied by a
436 composite inland Gondwana-derived source (Abbo et al., 2015; Dabard et al., 1996;
437 Denis and Dabard, 1988; Drost et al., 2011; Linnemann et al., 2014; Linnemann et al.,
438 2008; Orejana et al., 2015; Pereira et al., 2012a; Pereira et al., 2012b; Rabu et al.,
439 1990). However, there is no consensus on the relative extent of proximal vs. distal
440 supplies and the actual nature of the hinterland source. Several authors propose that
441 each peri-Gondwana terrane received distal detritus from specific domains of
442 Gondwana such as the Amazonian Craton, West African Craton, Saharan Metacraton
443 and Arabian Nubian Shield (Dörr et al., 2015; Henderson et al., 2016; Stephan et al.,
444 2018). Yet, the case of the Lower Gneiss Unit of the EFMC is still disputed as
445 Henderson et al. (2016) and Stephan et al. (2018) argue for a West African Craton
446 supply while Chelle-Michou et al. (2017) retain a Saharan Metacraton provenance. In
447 addition, none of those authors discuss the extent to which the erosion of the
448 Cadomian magmatic arc contributed to the observed detrital zircon age distributions in
449 the EFMC. In this section, we therefore (i) review the geological and isotopic
450 characteristics of the Cadomian arc and address its potential implication as a proximal
451 source for the Ediacaran EFMC sediments; and (ii) further discuss the nature of the
452 distal source based on the newly obtained, extensive dataset.

453

454 The largest and best preserved exposures of the Cadomian magmatic arc crop out in
455 the northern Armorican Massif (France and British Channel Islands, see Ballèvre et al.
456 (2001); Brown (1995); Chantraine et al. (2001); Strachan et al. (1996)). Even though
457 the exposed rocks may not correspond to those eroded at Ediacaran times, they can
458 still provide constraints on the nature, age pattern and isotopic signature of the
459 proximal detritus. In this crust segment, igneous rocks include: (i) late Cryogenian to
460 early Ediacaran (660–560 Ma) calc-alkaline suites comprising basic, intermediate and
461 acid components with radiogenic to unradiogenic Nd–Hf isotope signatures, taken as
462 evidence for arc–back-arc magmatism; (ii) late Ediacaran migmatites and peraluminous
463 granitoids (the Mancellian batholith, 560–540 Ma), proposed to have been generated
464 during back-arc basin inversion and resulting arc–continent collision. Scarce
465 Paleoproterozoic and Tonian crustal rocks (Icartian and Pentevrian gneisses,
466 respectively) are also documented. Figure **8a,b** presents a compilation of intrusion
467 ages available for igneous rocks from the northern Armorican Massif and obtained via
468 different geochronological methods (zircon and monazite U–Pb dating by LA–ICP–MS,
469 SIMS, EPMA and TIMS on single grains or multi-grain fractions for the latter technique,
470 whole-rock Rb–Sr). The observed age populations (540–750, c. 1800 and 2000–2200
471 Ma) are partly consistent with the spread of U–Pb dates in the detrital zircon record of
472 the EFMC. Importantly, the two subpeaks at 585 and 615 Ma observed in the latter
473 perfectly match the igneous dataset. Magmatic rocks emplaced in the time period 625-
474 750 Ma are present, but scarce in the Armorican Massif. This may reflect either a
475 sampling bias or the fact that Cadomian subduction and related magmatism were not
476 yet active at that time (as suggested by the Cadomian geological record elsewhere in
477 Europe, e.g. Garfunkel (2015)). The εHf(t) of various Cadomian intrusions are depicted
478 in figure **8c** (from Hf isotope studies or recalculated from Nd isotopes based on the
479 relation $\varepsilon Hf(t) = 1.36\ \varepsilon Nd(t) + 3$ determined by Vervoort et al. (1999)). Magmas

480 emplaced in the time period 750–620 Ma have supra-chondritic, DM-like Hf isotope
481 signatures. A clear shift towards less radiogenic source compositions occurred in the
482 Ediacaran, as magmas younger than 620 Ma show a broad range of inferred εHf(t)
483 from +5 down to sub-chondritic values of -11. In general, a large spread of radiogenic
484 isotope signatures at a given time period is interpreted to reflect the contamination of
485 juvenile magmas by old crustal remnants via AFC-type processes and/or magma or
486 source mixing as observed in many arcs built up on ancient continental crust (Bolhar et
487 al., 2008; Kelemen et al., 2003; Kemp et al., 2006).
488 Such a pattern is similar to that observed in the detrital zircon record of metasediments
489 from the Lower Gneiss Unit, yet slightly offset in time (to younger ages in the case of
490 Armorican rocks, Fig. **8c**). The case of Tonian–Stenian, Paleoproterozoic and Archean
491 zircon grains is more problematic as there are no rocks of such ages or appropriate
492 isotopic signatures in the Armorican Massif. There, Paleoproterozoic granitoids have
493 suprachondritic, DM-like, εHf(t) which are more elevated than those observed in detrital
494 zircons from the EFMC Ediacaran (meta)sediments (Fig. **8c**). Altogether, these
495 observations indicate that, our present state of knowledge, erosion of the Cadomian
496 arc *alone* unsatisfactorily explains the U–Pb–Hf systematics of the EFMC detritus thus
497 calling for the existence of an additional zircon source i.e. the main Gondwana land
498 (Drost et al., 2011; Linnemann et al., 2014; Linnemann et al., 2008; Orejana et al.,
499 2015; Pereira et al., 2012a; Pereira et al., 2012b).
500
501 By the mid-Ediacaran, the northern part of Gondwana had just been assembled and
502 stabilized following the late Cryogenian–Ediacaran Pan African orogenies (see
503 Garfunkel (2015)). The Gondwana crust (Fig. **9**) typically comprises cratonic domains
504 of Paleoproterozoic to Archean age (West African, Congo, Chad, Al Kufrah, Murzuq
505 cratons, see Liégeois et al. (2013)) and several Pan African mobile belts (Anti-Atlas,
506 Trans-Sahara and Oubanguides belts, East African orogen, Saharan Metacraton).

Most Pan African belts are composed of reworked cratonic crust ("metacraton") and remnants of 850–620 Ma-old subduction zone-type magmatic activity (oceanic arc accretion, continental arc systems) predating voluminous syn- to post-collisional magmatism at 620–570 Ma (Caby, 2003; Liégeois et al., 2003; Triantafyllou et al., 2016). Remobilization of ancient Paleoproterozoic to Archean crust is notably fingerprinted by the highly variable εNd(t) displayed by Ediacaran to late Cryogenian igneous rocks from the Trans-Sahara (Liégeois et al., 1998; Liégeois et al., 2003), Anti-Atlas (Errami et al., 2009), and Oubanguides (Toteu et al., 2001) belts. Only the Arabian-Nubian-Shield crust segment can be regarded as a juvenile Neoproterozoic terrane (Stern, 2002). In the following, we attempt to identify the areas that would have delivered distal detritus to the EFMC Ediacaran basins based on the igneous record of northern Gondwana.

Clearly, a supply from western African terranes must be disregarded because: (i) Paleoproterozoic rocks from the West African Craton have suprachondritic Hf isotope signatures whereas zircon grains of that age in the EFMC show a broad range of εHf(t) (Fig. **6**); (ii) Tonian rocks from the Trans-Sahara belt show subchondritic Nd isotope compositions (Liégeois et al., 1998) while the signature of Tonian EFMC grains points to a radiogenic source (Fig. **6**). An East African provenance encompassing erosion products from the Saharan Metacraton and the Arabian Nubian Shield is preferred for several reasons. First, early Cryogenian to Tonian igneous rocks in these areas are typified by suprachondritic Nd–Hf isotope signatures, matching the detrital record of the EFMC (Küster and Liégeois, 2001; Küster et al., 2008; Morag et al., 2011; Morag et al., 2012; Stern et al., 2010). Second, the sole fragments of late Stenian crust in north Gondwana have been described in the northern part of the Arabian Nubian Shield (Be'eri-Shlevin et al., 2012) and could represent the source of EFMC late Stenian zircon grains. Third, the zircon U–Pb–Hf systematics of recent detritus carried along by

534 the Nile river strikingly resemble the Ediacaran detrital zircon record of the EFMC (Fig.
535 **8d**) with two Neoproterozoic vertical arrays (550–650 and 950–1050 Ma), early
536 Cryogenian to Tonian radiogenic detritus (650–950 Ma) and adequate (largely sub-
537 chondritic) range of εHf(t) for the Paleoproterozoic and Archean grains (Be'eri-Shlevin
538 et al., 2014; Iizuka et al., 2013). As the river largely drains the eastern part of the
539 Sahara Metacraton and the Arabian Nubian Shield, we propose that the distal detritus
540 that fed the EFMC Ediacaran basin was sourced from both of these crustal domains.
541
542 Constraining the relative proportions of proximal vs. distal supplies within the EFMC
543 basin has proven ambiguous. The 0.65–1.0 and older-than-1.8 Ga zircon populations
544 most likely originate from erosion of the Sahara Metacraton/Arabian Nubian Shield but
545 the case of 0.55–0.65 Ga grains is controversial as both the Cadomian arc and the Pan
546 African mobile belts represent adequate suppliers. Nonetheless in this case and as
547 shown above, the Cadomian arc can only contribute to the 0.58-0.61 Ga zircons since
548 magmatic activity in the Armorican Massif peaked at that time (Fig. **8b**). Finally,
549 variations in the proportions of 0.55–0.65, 0.65–1.0 and older-than-1.8 Ga grains
550 among EFMC metasediments (see section 5.2) possibly reflect temporal changes in
551 the Saharan Metacraton vs. Arabian Nubian Shield distal inputs. When Sahara
552 Metacraton supplies were dominant, Ediacaran detritus would have featured abundant
553 older-than-1.8 Ga grains (Meinhold et al., 2011), and led to a zircon U–Pb–Hf pattern
554 akin to sample TN46. In contrast, preferential erosion of the Arabian Nubian Shield
555 would have delivered substantial amounts of 0.65–1.0 Ga grains (Morag et al., 2011;
556 Morag et al., 2012; Stern et al., 2010) and resulted in a pattern similar to that of sample
557 PdB16-01.
558
559 ## 5.4 Crustal evolution of the EFMC and the North Gondwana margin

560

561 The Ediacaran (590–545 Ma) deposition of the Lower Gneiss Unit metasediments
562 stamps the formation of the earliest crustal rocks so far known in the EFMC. The
563 nature (and even existence) of the basement on which the sediments were deposited
564 remains elusive as the EFMC crust segment typically lacks any remnant of pre-
565 Neoproterozoic rocks, neither at surface level (Chelle-Michou et al., 2017; Melleton et
566 al., 2010; Padel et al., 2017; Roques et al., 1995) nor in the lower crustal xenoliths
567 sampled by Cenozoic volcanoes (Féménias et al., 2003; Rossi et al., 2006).
568 Examination of the detrital zircon U–Pb–Hf signature indicates that the Ediacaran
569 basins collected detritus from the adjacent Cadomian magmatic arc and distal sources
570 from eastern Africa (see previous sections). Consequently, the EFMC crust segment
571 grew in the Ediacaran by pilling up pre-existing, eroded crustal materials of much
572 contrasted ancestries. From a crust evolution perspective, it is critical to establish the
573 relative proportions of eroded juvenile Neoproterozoic vs. old
574 Paleoproterozoic/Archean materials within the earliest EFMC crust as this would
575 constrain in turn the mechanisms and extent of Neoproterozoic crust production along
576 the North Gondwana margin. Importantly, assessing the amount of young crust based
577 on the proportion of detrital zircon grains showing radiogenic Hf isotope signatures is
578 not relevant because: (i) the low zircon fertility of arc rocks and their tendency to show
579 concordant U–Pb dates (see Dickinson (2008); Moecher and Samson (2006))
580 introduce sampling biases, and; (ii) grains showing unradiogenic Hf isotope signatures
581 but crystallized from hybrid crust–mantle magmas may still encapsulate a juvenile
582 component diluted by the non-stoichiometric incorporation of ancient crustal Hf (Bolhar
583 et al., 2008; Couzinié et al., 2016; Kemp et al., 2006). This is likely the case of
584 unradiogenic Ediacaran–early Cryogenian grains from the EFMC (see section 5.3).
585

586 By contrast, S-type (meta)granites of the Velay Orthogneiss Formation may provide a
587 more reliable probe of the actual amount of Cadomian juvenile detritus within the
588 Ediacaran basins. Following Couzinié et al. (2017), the (meta)granites indeed originate
589 from melting of the Ediacaran metasediments. These rocks show strikingly
590 homogeneous chondritic Hf isotope signatures, which resulted from dissolution of
591 detrital zircon grains and homogenization of their disparate Hf isotope signatures prior
592 to magma emplacement. If true, this model entails that the (meta)granites average the
593 Hf isotope composition of their Ediacaran sedimentary source. Earlier work pointed out
594 three main events of juvenile crust formation (i.e. with DM-like Hf-Nd isotope
595 signatures) in the Gondwanian realm, in the Neoproterozoic (i.e. Cadomian and ANS-
596 like, c. 0.65 Ga-old), Paleoproterozoic (Eburnean, c. 2.1 Ga-old) and Neoarchean (c.
597 2.8 Ga-old) (Gerdes and Zeh, 2006; Kemp et al., 2006; Linnemann et al., 2014;
598 Orejana et al., 2015). Therefore, the Hf isotopic composition of the Ediacaran
599 sediments can be viewed as a mixture of those three components in different
600 proportions – in turn sampled by the Velay Orthogneiss Formation (meta)granites.
601 Following this, the chondritic signature of the latter demands that 60–75 % of the
602 Ediacaran detritus in the EFMC corresponds to newly formed (i.e. <100 Ma-old) and
603 isotopically juvenile Neoproterozoic crust (Fig. **10**), either formerly part of the Cadomian
604 arc or originating from eastern Africa. This first-order estimate is minimal because
605 newly formed Neoproterozoic crust did not necessarily show a DM-like Hf isotope
606 composition. Several studies indeed documented that the very limited incorporation of
607 recycled crustal materials in the mantle source of arc and post-collisional magmas can
608 shift their Hf isotope composition towards non DM-like values (Nebel et al., 2011;
609 Roberts et al., 2012).
610
611 Interestingly, similar estimates can be obtained from the isotopic signature of several
612 late Ediacaran–early Paleozoic S-type granites from the North Gondwana margin, all

presumably derived from melting of Ediacaran sediments. In the Bohemian Massif, magmatic zircons from the c. 540 Ma-old Laubach granite (Linnemann et al., 2014) show a tight range of εHf(t) at 0 ± 2.4 ε-units (1 S.D.), identical to that of the Velay Orthogneiss Formation (meta)granites. In the Iberian Massif, the Cambrian–Ordovician volcano-plutonic Ollo de Sapo formation also displays an average εHf(t) of 0 ± 4.1 ε-units (1 S.D.) (Montero et al., 2017) whereas in both areas detrital zircons from Ediacaran sediments feature a very wide range of εHf(t), spanning over 30 to 40 ε-units (Linnemann et al., 2014; Linnemann et al., 2017; Orejana et al., 2015). Such observations further support the claim that late Ediacaran intra-arc or back-arc basins developed along the North Gondwana margin largely represent newly formed continental crust as they were primarily fed by detritus originating from <100 Ma-old, Neoproterozoic terranes.

6. Conclusion

In this study, we demonstrate that the Lower Gneiss Unit of the eastern French Massif Central, a portion of the internal (Moldanubian) zone of the late Paleozoic Variscan collisional orogen, encompasses Ediacaran siliciclastic sedimentary successions metamorphosed in the amphibolite-facies at Variscan times. Statistical analysis of detrital zircon U–Pb date distributions reveals that the Lower Gneiss Unit crust segment had a distinct Ediacaran paleogeographic position with respect to adjacent Variscan massifs (Central Iberian Zone, Bohemian Massif, Armorican Massif). Coupled zircon U–Pb–Hf systematics, notably the highly diverse Hf isotope composition displayed by Ediacaran to late Cryogenian individual grains, can be reconciled with Ediacaran detritus being collected from the adjacent Cadomian continental arc plus additional hinterland supplies from eastern African sources (Sahara Metacraton and

Arabian Nubian Shield). A dominant proportion of the detritus (60–75% according to our first-order, minimal estimates) represents fragments of Neoproterozoic crustal materials extracted from the mantle shortly prior to erosion, transport and sedimentation in the Ediacaran basins of the EFMC. Therefore, even though substantial amounts of genuine mantle-derived Neoproterozoic igneous rocks experienced sedimentary reworking and were not preserved, their erosion products were collected in an (attenuated) crustal environment (the intra-arc or back-arc basins) and became de facto long-term additions to the continental crust volume. Importantly, the existence of concomitant sedimentary inputs from distal cratonic sources and the incorporation of old crustal materials in continental arc magmas resulted in this newly formed crust being intrinsically heterogeneous from an Hf isotope perspective. Several studies argued that a scatter in the zircon εHf(t) at a given time period, as observed in the Ediacaran–Cryogenian record of the North Gondwana margin, reflects the dominance of crust reworking processes (Dhuime et al., 2017; Kemp et al., 2006; Vervoort and Kemp, 2016). In contrast, this work shows that such a situation may just as well reflect voluminous new crust production.

Acknowledgements

C. Guilbaud made the thin sections; J.-M. Hénot assisted during SEM imaging; M. Ballèvre provided the file of Fig. 1; M. Mintrone contributed to Fig. 2; A. Laurent, A. Vezinet, A. Villaros, V. Gardien and G. Mahéo participated to stimulating discussions; C. Storey, U. Linnemann and an anonymous reviewer substantially improved the manuscript; may they all be thanked.

Figures captions

Figure 1: Sketch map of the crustal blocks involved in the Variscan orogeny, adapted from Ballevre et al. (2014). Yellow stars highlight the location of detrital zircon studies performed on Ediacaran–Lower Cambrian (meta)sediments and considered section 5.2. Zones: CIZ, Central Iberian; CZ, Cantabrian; GTMZ, Galicia–Trás-os-Montes; OMZ, Ossa-Morena; RHZ, Rheno-Hercynian; SPZ, South-Portuguese; STZ, Saxo-Thuringian; TBZ, Teplá-Barrandian; WALZ, West Asturian–Leonese. VF: Variscan Front. References: 1, Linnemann et al. (2007); 2, Linnemann et al. (2014); 3, Linnemann et al. (2017); 4, Drost et al. (2011); 5, Hajná et al. (2017); 6, Žák and Sláma (2017); 7, Fernández-Suárez et al. (2014); 8, Naidoo et al. (2017) ; 9, Zimmermann et al. (2015); 10, Díez Fernández et al. (2010); 11, Orejana et al. (2015) ; 12, Pereira et al. (2012b) ; 13, Pereira et al. (2012a) ; 14, Talavera et al. (2012); 15, Teixeira et al. (2011); 16, Ballouard (2016) ; 17, Gougeon et al. (2017); 18, Padel et al. (2017); 19, Chelle-Michou et al. (2017).

Figure 2: Geological map of the Velay dome area showing the location of analyzed metasediments. The extent of Variscan partial melting of the metamorphic lithologies is not shown for sake of clarity. Redrawn after Ledru et al. (2001) and regional geological maps of France at scale 1/50000.

Figure 3: Representative cathodoluminescence images of zircon grains from Lower Gneiss Unit metasediments. The locations of laser spots (white and yellow circles for U-Pb and Lu-Hf analyses respectively) are indicated along with the spot name (zXX or #YY). The corresponding $^{206}Pb/^{238}U$ dates (if <1.2 Ga) or $^{207}Pb/^{206}Pb$ dates (if >1.2 Ga) are quoted with 2σ uncertainty, in Ma. All displayed analyses are concordant at >95%.

690 Hf isotope data are reported using the εHf calculated at the $^{206}Pb/^{238}U$ or $^{207}Pb/^{206}Pb$
691 date obtained on the same zircon domain, quoted with 2σ uncertainty.
692
693 Figure 4: Tera–Wasserburg diagrams ($^{238}U/^{206}Pb$ vs. $^{207}Pb/^{206}Pb$) showing
694 Neoproterozoic zircon data for the Lower Gneiss Unit metasediments. Error
695 ellipses/ages are quoted at 2σ level of uncertainty. Colored ellipses are those included
696 in Concordia age calculations. Dotted ellipses for TN46 refer to data from Chelle-
697 Michou et al. (2017).
698
699 Figure 5: Zircon U–Pb date distribution of investigated metasediments from the Lower
700 Gneiss Unit represented as Kernel Density Estimates (KDE). Only 95–105%
701 concordant $^{206}Pb/^{238}U$ (for dates < 1.2 Ga) and $^{207}Pb/^{206}Pb$ dates (for dates > 1.2 Ga)
702 were considered. Circles below the x-axis are the central value of individual data
703 points. Plotted with the DensityPlotter program of Vermeesch (2012) using an adaptive
704 bandwidth.
705
706 Figure 6: Combined U-Pb and Lu-Hf isotopic data for zircons from Ediacaran
707 metasediments, constituent rocks of the Lower Gneiss Unit in the Eastern French
708 Massif Central. The data for sample TN46 are from Chelle-Michou et al. (2017). The
709 εHf(t) range for the Depleted Mantle reservoir is bracketed by the models of Naeraa et
710 al. (2012) and Griffin et al. (2002). The dotted arrow represents the isotopic evolution of
711 continental crust (calculated using an average crustal $^{176}Lu/^{177}Hf$ ratio of 0.0113).
712
713 Figure 7: (a) Non-metric multi-dimensional scaling plot of the Ediacaran–Lower
714 Cambrian (meta)sedimentary dataset comprising 54 samples from several zones of the
715 Variscan belt. Samples from the Ossa-Morena zone (n=2) are not depicted for sake of
716 clarity. See section 5.3 for details on the calculations. (b) Same plot on which the zircon

U–Pb date distributions of four selected samples from the literature are displayed with the aim to highlight the end-member zircon populations.

Figure 8: (a–b) Available intrusion ages for igneous rocks older than 550 Ma in the northern Armorican Massif compared to the detrital zircon record of the Lower Gneiss Unit in the Eastern French Massif Central, represented as Kernel Density Estimates (KDE). Only 95–105% concordant $^{206}Pb/^{238}U$ (for dates < 1.2 Ga) and ^{207}Pb ^{206}Pb dates (for dates > 1.2 Ga) were considered. Plotted with the DensityPlotter program of Vermeesch (2012) with an adaptive bandwidth. Geochronological data for the Armorican Massif were extracted from the compilation of Thiéblemont et al. (2017) supplemented by results from Inglis et al. (2005); Inglis et al. (2004) and Vidal (1980). (c) Hf isotope signature of igneous rocks from the northern Armorican Massif (from Hf isotope studies or recalculated from Nd isotopes based on the relation $\varepsilon Hf(t) = 1.36\ \varepsilon Nd(t) + 3$ determined by Vervoort et al. (1999)) compared to the detrital zircon record of the EFMC. Data from D'Lemos and Brown (1993); Dabard et al. (1996); Guerrot (1989); Samson and D'Lemos (1998); Samson et al. (2003). (d) U–Pb/Lu–Hf systematics of detrital zircon grains from recent sediments of the Nile River, taken as representative of the eastern part of the Sahara Metacraton and western part of the Arabian Nubian Shield, compared to the EFMC record. Data from Be'eri-Shlevin et al. (2014) and Iizuka et al. (2013).

Figure 9: Geological sketch of the northern part of the Gondwana by the late Ediacaran (c. 560 Ma) delineating the main crustal domains (age and Nd–Hf isotope signature) representing putative zircons sources for the EFMC detritus. Arrows represent the likely sources of the detrital supply that fed the Ediacaran EFMC basin. Inspired from Garfunkel (2015) and references therein.

Figure 10: Triangular diagram showing εHf(545 Ma) of a virtual sedimentary material as a function of the relative proportions of juvenile Neoproterozoic (Cadomian and ANS-like), Paleoproterozoic (Eburnean) and Neoarchean crust in the latter, assuming identical Hf concentrations in the three end-members. The εHf(545 Ma) of each component was calculated based on a $^{176}Lu/^{177}Hf$ of 0.0113 and extraction from a DM source (considering the average value of the models from Griffin et al. (2002) and Naeraa et al. (2012)). The highlighted value of zero corresponds to the average composition of the Ediacaran metasediments required to explain the zircon Hf isotope signature of the Velay Orthogneiss Formation (and other pre-Variscan granitoids emplaced at the Ediacaran-Cambrian boundary, see text for details).

References

Abbo, A., Avigad, D., Gerdes, A., Güngör, T., 2015. Cadomian basement and Paleozoic to Triassic siliciclastics of the Taurides (Karacahisar dome, south-central Turkey): Paleogeographic constraints from U–Pb–Hf in zircons. Lithos 227, 122-139.

Ballèvre, M., Le Goff, E., Hébert, R., 2001. The tectonothermal evolution of the Cadomian belt of northern Brittany, France: a Neoproterozoic volcanic arc. Tectonophysics 331, 19-43.

Ballouard, C., 2016. Origine, évolution et exhumation des leucogranites peralumineux de la chaîne hercynienne armoricaine : implication sur la métallogénie de l'uranium. Rennes.

Be'eri-Shlevin, Y., Eyal, M., Eyal, Y., Whitehouse, M.J., Litvinovsky, B., 2012. The Sa'al volcano-sedimentary complex (Sinai, Egypt): A latest Mesoproterozoic volcanic arc in the northern Arabian Nubian Shield. Geology 40, 403-406.

769 Be'eri-Shlevin, Y., Avigad, D., Gerdes, A., Zlatkin, O., 2014. Detrital zircon U–Pb–Hf
770 systematics of Israeli coastal sands: new perspectives on the provenance of Nile
771 sediments. Journal of the Geological Society 171, 107-116.
772 Bolhar, R., Weaver, S.D., Whitehouse, M.J., Palin, J.M., Woodhead, J.D., Cole, J.W.,
773 2008. Sources and evolution of arc magmas inferred from coupled O and Hf isotope
774 systematics of plutonic zircons from the Cretaceous Separation Point Suite (New
775 Zealand). Earth and Planetary Science Letters 268, 312-324.
776 Borg, I., Groenen, P.J., 2005. Modern Multidimensional Scaling: Theory and
777 Applications. Springer.
778 Briand, B., Combémorel, R., Couturié, J.-P., Bérard, P., Vautrelle, C., 1993. Notice
779 explicative, Carte géol. France (1/50 000), feuille Le Bleymard (863). BRGM, Orléans.
780 Brown, M., 1995. The late-Precambrian geodynamic evolution of the Armorica segment
781 of the Cadomian belt (France): Distortion of an active continental margin during south-
782 west directed convergence and subduction of a bathymetric high. Géologie de la
783 France 3, 3-22.
784 Caby, R., 2003. Terrane assembly and geodynamic evolution of central–western
785 Hoggar: a synthesis. Journal of African Earth Sciences 37, 133-159.
786 Cawood, P.A., Kröner, A., Collins, W.J., Kusky, T.M., Mooney, W.D., Windley, B.F.,
787 2009. Accretionary orogens through Earth history. Geological Society, London, Special
788 Publications 318, 1-36.
789 Chantraine, J., Egal, E., Thiéblemont, D., Le Goff, E., Guerrot, C., Ballèvre, M.,
790 Guennoc, P., 2001. The Cadomian active margin (Northern Armorican Massif, France):
791 a segment of the North Atlantic Panafrican belt. Tectonophysics 331, 1-18.
792 Chelle-Michou, C., Laurent, O., Moyen, J.-F., Block, S., Paquette, J.-L., Couzinié, S.,
793 Gardien, V., Vanderhaeghe, O., Villaros, A., Zeh, A., 2017. Pre-Cadomian to late-
794 Variscan odyssey of the eastern Massif Central, France: Formation of the West
795 European crust in a nutshell. Gondwana Research 46, 170-190.

796 Condie, K.C., Aster, R.C., 2010. Episodic zircon age spectra of orogenic granitoids:
797 The supercontinent connection and continental growth. Precambrian Research 180,
798 227-236.
799 Couzinié, S., Laurent, O., Moyen, J.F., Zeh, A., Bouilhol, P., Villaros, A., 2016. Post-
800 collisional magmatism: Crustal growth not identified by zircon Hf-O isotopes. Earth and
801 Planetary Science Letters 456, 182-195.
802 Couzinié, S., Laurent, O., Poujol, M., Mintrone, M., Chelle-Michou, C., Moyen, J.-F.,
803 Bouilhol, P., Vezinet, A., Marko, L., 2017. Cadomian S-type granites as basement
804 rocks of the Variscan belt (Massif Central, France): Implications for the crustal
805 evolution of the north Gondwana margin. Lithos 286-287, 16-34.
806 Couzinié, S., Moyen, J.F., Villaros, A., Paquette, J.L., Scarrow, J.H., Marignac, C.,
807 2014. Temporal relationships between Mg-K mafic magmatism and catastrophic
808 melting of the Variscan crust in the southern part of Velay Complex (Massif Central,
809 France). Journal of GEOsciences, 69-86.
810 D'Lemos, R.S., Brown, M., 1993. Sm–Nd isotope characteristics of late Cadomian
811 granite magmatism in northern France and the Channel Islands. Geological Magazine
812 130, 797-804.
813 Dabard, M.P., Loi, A., Peucat, J.J., 1996. Zircon typology combined with Sm-Nd whole-
814 rock isotope analysis to study Brioverian sediments from the Armorican Massif.
815 Sedimentary Geology 101, 243-260.
816 Denis, E., Dabard, M.P., 1988. Sandstone petrography and geochemistry of late
817 Proterozoic sediments of the Armorican Massif (France) – A key to basin development
818 during the Cadomian orogeny Precambrian Research 42, 189-206.
819 Dhuime, B., Hawkesworth, C.J., Delavault, H., Cawood, P.A., 2017. Continental growth
820 seen through the sedimentary record. Sedimentary Geology 357, 16-32.

821 Dickinson, W.R., 2008. Impact of differential zircon fertility of granitoid basement rocks
822 in North America on age populations of detrital zircons and implications for granite
823 petrogenesis. Earth and Planetary Science Letters 275, 80-92.
824 Díez Fernández, R., Catalán, J.R.M., Gerdes, A., Abati, J., Arenas, R., Fernández-
825 Suárez, J., 2010. U–Pb ages of detrital zircons from the Basal allochthonous units of
826 NW Iberia: Provenance and paleoposition on the northern margin of Gondwana during
827 the Neoproterozoic and Paleozoic. Gondwana Research 18, 385-399.
828 Dörr, W., Zulauf, G., Gerdes, A., Lahaye, Y., Kowalczyk, G., 2015. A hidden Tonian
829 basement in the eastern Mediterranean: Age constraints from U–Pb data of magmatic
830 and detrital zircons of the External Hellenides (Crete and Peloponnesus). Precambrian
831 Research 258, 83-108.
832 Drost, K., Gerdes, A., Jeffries, T., Linnemann, U., Storey, C., 2011. Provenance of
833 Neoproterozoic and early Paleozoic siliciclastic rocks of the Teplá-Barrandian unit
834 (Bohemian Massif): Evidence from U–Pb detrital zircon ages. Gondwana Research 19,
835 213-231.
836 Errami, E., Bonin, B., Laduron, D., Lasri, L., 2009. Petrology and geodynamic
837 significance of the post-collisional Pan-African magmatism in the Eastern Saghro area
838 (Anti-Atlas, Morocco). Journal of African Earth Sciences 55, 105-124.
839 Faure, M., Brouder, P., Thierry, J., Alabouvette, B., Cocherie, A., Bouchot, V., 2009a.
840 Notice explicative, Carte géol. France (1/50 000), feuille Saint-André-de-Valborgne
841 (911). BRGM, Orléans.
842 Faure, M., Lardeaux, J.-M., Ledru, P., 2009b. A review of the pre-Permian geology of
843 the Variscan French Massif Central. Comptes Rendus Geoscience 341, 202-213.
844 Féménias, O., Coussaert, N., Bingen, B., Whitehouse, M., Mercier, J.-C.C., Demaiffe,
845 D., 2003. A Permian underplating event in late- to post-orogenic tectonic setting.
846 Evidence from the mafic–ultramafic layered xenoliths from Beaunit (French Massif
847 Central). Chemical Geology 199, 293-315.

848 Fernández-Suárez, J., Gutiérrez Alonso, G., Pastor-Galán, D., Hofmann, A.W.,
849 Murphy, J.B., Linnemann, U., 2014. The Ediacaran–Early Cambrian detrital zircon
850 record of NW Iberia: possible sources and paleogeographic constraints. International
851 Journal of Earth Sciences 103, 1335-1357.
852 Feybesse, J.-L., Lardeaux, J.M., Tegyey, M., Peterlongo, J.-M., Kerrien, Y., Lemière,
853 B., Maurin, G., Mercier, F., Thiéblemont, D., 1995. Notice explicative, Carte géol.
854 France (1/50 000), feuille Saint-Symphorien-sur-Coise (721). BRGM, Orléans.
855 Franke, W., 1989. Variscan plate tectonics in Central Europe - current ideas and open
856 questions. Tectonophysics 169, 221-228.
857 Gardien, V., 1990. Reliques de grenat et de staurotide dans la série métamorphique de
858 basse pression du Mont Pilat (Massif Central français) : témonis d'une évolution
859 tectonométamorphique polyphasée. Comptes Rendus de l'Académie des Sciences,
860 Paris 310, 233-240.
861 Garfunkel, Z., 2015. The relations between Gondwana and the adjacent peripheral
862 Cadomian domain—constrains on the origin, history, and paleogeography of the
863 peripheral domain. Gondwana Research 28, 1257-1281.
864 Gerdes, A., Zeh, A., 2006. Combined U–Pb and Hf isotope LA-(MC-)ICP-MS analyses
865 of detrital zircons: Comparison with SHRIMP and new constraints for the provenance
866 and age of an Armorican metasediment in Central Germany. Earth and Planetary
867 Science Letters 249, 47-61.
868 Gougeon, R., Néraudeau, D., Dabard, M.-P., Pierson-Wickmann, A.-C., Polette, F.,
869 Poujol, M., Saint-Martin, J.-P., 2017. Trace Fossils from the Brioverian (Ediacaran–
870 Fortunian) in Brittany (NW France). Ichnos, 1-14.
871 Griffin, W.L., Wang, X., Jackson, S.E., Pearson, N.J., O'Reilly, S.Y., Xu, X.-S., Zhou,
872 X., 2002. Zircon chemistry and magma mixing, SE China: In-situ analysis of Hf
873 isotopes, Tonglu and Pingtan igneous complexes. Lithos 61, 237-269.

874 Guerrot, C., 1989. Archéen et Protérozoïque dans la chaîne hercynienne ouest-
875 européenne, géochimie isotopique (Sr-Nd-Pb) et géochronologie U-Pb sur zircons.
876 Rennes, p. 206.
877 Hajná, J., Žák, J., Dörr, W., 2017. Time scales and mechanisms of growth of active
878 margins of Gondwana: A model based on detrital zircon ages from the Neoproterozoic
879 to Cambrian Blovice accretionary complex, Bohemian Massif. Gondwana Research 42,
880 63-83.
881 Henderson, B.J., Collins, W.J., Murphy, J.B., Gutierrez-Alonso, G., Hand, M., 2016.
882 Gondwanan basement terranes of the Variscan–Appalachian orogen: Baltican,
883 Saharan and West African hafnium isotopic fingerprints in Avalonia, Iberia and the
884 Armorican Terranes. Tectonophysics 681, 278-304.
885 Herron, M.M., 1988. Geochemical classification of terrigenous sands and shales from
886 core and log data. Journal of Sedimentary Petrology 58, 820-829.
887 Ihaka, R., Gentleman, R., 1996. R: a language for data analysis and graphics. Journal
888 of Computational and Graphical Statistics 5, 299-344.
889 Iizuka, T., Campbell, I.H., Allen, C.M., Gill, J.B., Maruyama, S., Makoka, F., 2013.
890 Evolution of the African continental crust as recorded by U–Pb, Lu–Hf and O isotopes
891 in detrital zircons from modern rivers. Geochimica et Cosmochimica Acta 107, 96-120.
892 Iizuka, T., Hirata, T., Komiya, T., Rino, S., Katayama, I., Motoki, A., Maruyama, S.,
893 2005. U-Pb and Lu-Hf isotope systematics of zircons from the Mississippi River sand:
894 Implications for reworking and growth of continental crust. Geology 33, 485.
895 Inglis, J.D., Samson, S.D., D'Lemos, R.S., Miller, B.V., 2005. Timing of Cadomian
896 deformation and magmatism within La Hague, NW France. Journal of the Geological
897 Society, London 162, 389-400.
898 Inglis, J.D., Samson, S.D., D'Lemos, R.S., Hamilton, M., 2004. U–Pb geochronological
899 constraints on the tectonothermal evolution of the Paleoproterozoic basement of
900 Cadomia, La Hague, NW France. Precambrian Research 134, 293-315.

Kelemen, P.B., Hanghoj, K., Greene, A.R., 2003. One view of the geochemistry of subduction-related magmatic arcs, withan emphasis on primitive andesite and lower crust, in: Rudnick, R.L. (Ed.), Treatise on Geochemistry. Elsevier, pp. 593-659.

Kemp, A.I., Hawkesworth, C.J., Paterson, B.A., Kinny, P.D., 2006. Episodic growth of the Gondwana supercontinent from hafnium and oxygen isotopes in zircon. Nature 439, 580-583.

Kroner, U., Romer, R.L., 2013. Two plates — Many subduction zones: The Variscan orogeny reconsidered. Gondwana Research 24, 298-329.

Küster, D., Liégeois, J.-P., 2001. Sr, Nd isotopes and geochemistry of the Bayuda Desert high-grade metamorphic basement (Sudan): an early Pan-African oceanic convergent margin, not the edge of the East Saharan ghost craton? Precambrian Research 109, 1-23.

Küster, D., Liégeois, J.-P., Matukov, D., Sergeev, S., Lucassen, F., 2008. Zircon geochronology and Sr, Nd, Pb isotope geochemistry of granitoids from Bayuda Desert and Sabaloka (Sudan): Evidence for a Bayudian event (920–900Ma) preceding the Pan-African orogenic cycle (860–590Ma) at the eastern boundary of the Saharan Metacraton. Precambrian Research 164, 16-39.

Lardeaux, J.M., Schulmann, K., Faure, M., Janou ek, V., Lexa, O., Skrzypek, E., Edel, J.B., tipska, P., 2014. The Moldanubian Zone in the French Massif Central, Vosges/Schwarzwald and Bohemian Massif revisited: differences and similarities. Geological Society, London, Special Publications 405, 7-44.

Laurent, O., Couzinié, S., Zeh, A., Vanderhaeghe, O., Moyen, J.-F., Villaros, A., Gardien, V., Chelle-Michou, C., 2017. Protracted, coeval crust and mantle melting during Variscan late-orogenic evolution: U–Pb dating in the eastern French Massif Central. International Journal of Earth Sciences 106, 421-451.

926 Ledru, P., Courrioux, G., Dallain, C., Lardeaux, J.M., Montel, J.M., Vanderhaeghe, O.,
927 Vitel, G., 2001. The Velay dome (French Massif Central): melt generation and granite
928 emplacement during orogenic evolution. Tectonophysics 342, 207-237.
929 Ledru, P., Lardeaux, J.M., Santallier, D., Autran, A., Quenardel, J.-M., Floc'h, J.-P.,
930 Lerouge, G., Maillet, N., Marchand, J., Ploquin, A., 1989. Where are the nappes in the
931 French Massif central? Bulletin de la Société Géologique de France 8, 605-618.
932 Ledru, P., Vitel, G., Marchand, J., Maurin, G., Mercier, F., Turland, M., Etlicher, B.,
933 Dautria, J.M., Liotard, J.M., 1994. Notice explicative, Carte géol. France (1/50 000),
934 feuille Craponne-sur-Arzon (767). BRGM, Orléans.
935 Liégeois, J.-P., Abdelsalam, M.G., Ennih, N., Ouabadi, A., 2013. Metacraton: Nature,
936 genesis and behavior. Gondwana Research 23, 220-237.
937 Liégeois, J.-P., Navez, J., Hertogen, J., Black, R., 1998. Contrasting origin of post-
938 collisional high-K calc-alkaline and shoshonitic versus alkaline and peralkaline
939 granitoids. The use of sliding normalization. Lithos 45, 1-28.
940 Liégeois, J.P., Latouche, L., Boughrara, M., Navez, J., Guiraud, M., 2003. The LATEA
941 metacraton (Central Hoggar, Tuareg shield, Algeria): behaviour of an old passive
942 margin during the Pan-African orogeny. Journal of African Earth Sciences 37, 161-190.
943 Linnemann, U., Gerdes, A., Drost, K., Buschmann, B., 2007. The continuum between
944 Cadomian orogenesis and opening of the Rheic Ocean: Constraints from LA-ICP-MS
945 U-Pb zircon dating and analysis of plate-tectonic setting (Saxo-Thuringian zone,
946 northeastern Bohemian Massif, Germany). 423, 61-96.
947 Linnemann, U., Gerdes, A., Hofmann, M., Marko, L., 2014. The Cadomian Orogen:
948 Neoproterozoic to Early Cambrian crustal growth and orogenic zoning along the
949 periphery of the West African Craton—Constraints from U–Pb zircon ages and Hf
950 isotopes (Schwarzburg Antiform, Germany). Precambrian Research 244, 236-278.
951 Linnemann, U., Pereira, F., Jeffries, T.E., Drost, K., Gerdes, A., 2008. The Cadomian
952 Orogeny and the opening of the Rheic Ocean: The diacrony of geotectonic processes

953 constrained by LA-ICP-MS U–Pb zircon dating (Ossa-Morena and Saxo-Thuringian
954 Zones, Iberian and Bohemian Massifs). Tectonophysics 461, 21-43.
955 Linnemann, U., Pidal, A.P., Hofmann, M., Drost, K., Quesada, C., Gerdes, A., Marko,
956 L., Gärtner, A., Zieger, J., Ulrich, J., Krause, R., Vickers-Rich, P., Horak, J., 2017. A
957 ~565 Ma old glaciation in the Ediacaran of peri-Gondwanan West Africa. International
958 Journal of Earth Sciences.
959 Lotout, C., Pitra, P., Poujol, M., Anczkiewicz, R., Van Den Driessche, J., 2018. Timing
960 and duration of Variscan high-pressure metamorphism in the French Massif Central: A
961 multimethod geochronological study from the Najac Massif. Lithos 308-309, 381-394.
962 Malavielle, J., Guihot, P., Costa, S., Lardeaux, J.M., Gardien, V., 1990. Collapse of the
963 thickened Variscan crust in the French Massif Central: Mont Pilat extensional shear
964 zone and St. Etienne Late Carboniferous basin. Tectonophysics 177, 139-149.
965 Matte, P., 1986. Tectonics and plate tectonics model for the Variscan belt of Europe.
966 Tectonophysics 126, 329-374.
967 Meinhold, G., Morton, A.C., Fanning, C.M., Frei, D., Howard, J.P., Phillips, R.J.,
968 Strogen, D., Whitham, A.G., 2011. Evidence from detrital zircons for recycling of
969 Mesoproterozoic and Neoproterozoic crust recorded in Paleozoic and Mesozoic
970 sandstones of southern Libya. Earth and Planetary Science Letters 312, 164-175.
971 Melleton, J., Cocherie, A., Faure, M., Rossi, P., 2010. Precambrian protoliths and Early
972 Paleozoic magmatism in the French Massif Central: U–Pb data and the North
973 Gondwana connection in the west European Variscan belt. Gondwana Research 17,
974 13-25.
975 Mintrone, M., 2016. Constraining the duration of metamorphic events by modeling of
976 phase equilibrium and diffusion in garnet. Example from the French Massif Central.
977 Clermont-Ferrand, p. 54.

978 Moecher, D., Samson, S., 2006. Differential zircon fertility of source terranes and
979 natural bias in the detrital zircon record: Implications for sedimentary provenance
980 analysis. Earth and Planetary Science Letters 247, 252-266.
981 Montel, J.M., Marignac, C., Barbey, P., Pichavant, M., 1992. Thermobarometry and
982 granite genesis: the Hercynian low-P, high-T Velay anatectic dome (French Massif
983 Central). Journal of Metamorphic Geology 10, 1-15.
984 Montero, P., Talavera, C., Bea, F., 2017. Geochemical, isotopic, and zircon (U-Pb, O,
985 Hf isotopes) evidence for the magmatic sources of the volcano-plutonic Ollo de Sapo
986 Formation, Central Iberia. Geologica Acta 15, 245-260.
987 Morag, N., Avigad, D., Gerdes, A., Belousova, E., Harlavan, Y., 2011. Crustal evolution
988 and recycling in the northern Arabian-Nubian Shield: New perspectives from zircon Lu–
989 Hf and U–Pb systematics. Precambrian Research 186, 101-116.
990 Morag, N., Avigad, D., Gerdes, A., Harlavan, Y., 2012. 1000–580 Ma crustal evolution
991 in the northern Arabian-Nubian Shield revealed by U–Pb–Hf of detrital zircons from late
992 Neoproterozoic sediments (Elat area, Israel). Precambrian Research 208-211, 197-
993 212.
994 Mougeot, R., Respaut, J.P., Ledru, P., Marignac, C., 1997. U-Pb chronology on
995 accessory minerals of the Velay anatectic dome (French Massif Central). European
996 Journal of Mineralogy 9, 141-156.
997 Murphy, J.B., Nance, R.D., 1989. Model for the evolution of the Avalonian-Cadomian
998 belt. Geology 17, 735.
999 Murphy, J.B., Pisarevsky, S.A., Nance, R.D., Keppie, J.D., 2004. Neoproterozoic-Early
1000 Paleozoic evolution of peri-Gondwanan terranes: implications for Laurentia-Gondwana
1001 connections. International Journal of Earth Sciences 93, 659-682.
1002 Naeraa, T., Schersten, A., Rosing, M.T., Kemp, A.I., Hoffmann, J.E., Kokfelt, T.F.,
1003 Whitehouse, M.J., 2012. Hafnium isotope evidence for a transition in the dynamics of
1004 continental growth 3.2 Gyr ago. Nature 485, 627-630.

1005 Nagy, E.A., Samson, S.D., D'Lemos, R.S., 2002. U–Pb geochronological constraints
1006 on the timing of Brioverian sedimentation and regional deformation in the St. Brieuc
1007 region of the Neoproterozoic Cadomian orogen, northern France. Precambrian
1008 Research 116, 1-17.
1009 Naidoo, T., Zimmermann, U., Vervoort, J., Tait, J., 2017. Evidence of early Archean
1010 crust in northwest Gondwana, from U–Pb and Hf isotope analysis of detrital zircon, in
1011 Ediacaran surpacrustal rocks of northern Spain. International Journal of Earth
1012 Sciences.
1013 Nebel, O., Vroon, P.Z., van Westrenen, W., Iizuka, T., Davies, G.R., 2011. The effect of
1014 sediment recycling in subduction zones on the Hf isotope character of new arc crust,
1015 Banda arc, Indonesia. Earth and Planetary Science Letters 303, 240-250.
1016 Orejana, D., Merino Martínez, E., Villaseca, C., Andersen, T., 2015. Ediacaran–
1017 Cambrian paleogeography and geodynamic setting of the Central Iberian Zone:
1018 Constraints from coupled U–Pb–Hf isotopes of detrital zircons. Precambrian Research
1019 261, 234-251.
1020 Padel, M., Álvaro, J.J., Clausen, S., Guillot, F., Poujol, M., Chichorro, M., Monceret, É.,
1021 Pereira, M.F., Vizcaïno, D., 2017. U–Pb laser ablation ICP-MS zircon dating across the
1022 Ediacaran–Cambrian transition of the Montagne Noire, southern France. Comptes
1023 Rendus Geoscience.
1024 Pereira, M., Chichorro, M., Linnemann, U., Eguiluz, L., Silva, J., 2006. Inherited arc
1025 signature in Ediacaran and Early Cambrian basins of the Ossa-Morena Zone (Iberian
1026 Massif, Portugal): Paleogeographic link with European and North African Cadomian
1027 correlatives. Precambrian Research 144, 297-315.
1028 Pereira, M.F., 2014. Potential sources of Ediacaran strata of Iberia: a review.
1029 Geodinamica Acta 27, 1-14.
1030 Pereira, M.F., Linnemann, U., Hofmann, M., Chichorro, M., Solá, A.R., Medina, J.,
1031 Silva, J.B., 2012a. The provenance of Late Ediacaran and Early Ordovician siliciclastic

1032 rocks in the Southwest Central Iberian Zone: Constraints from detrital zircon data on
1033 northern Gondwana margin evolution during the late Neoproterozoic. Precambrian
1034 Research 192-195, 166-189.
1035 Pereira, M.F., Solá, A.R., Chichorro, M., Lopes, L., Gerdes, A., Silva, J.B., 2012b.
1036 North-Gondwana assembly, break-up and paleogeography: U–Pb isotope evidence
1037 from detrital and igneous zircons of Ediacaran and Cambrian rocks of SW Iberia.
1038 Gondwana Research 22, 866-881.
1039 Rabu, D., Chantraine, J., Chauvel, J.J., Denis, E., Balé, P., Bardy, P., 1990. The
1040 Brioverian (Upper Proterozoic) and the Cadomian orogeny in the Armorican Massif, in:
1041 D'Lemos, R.S., Strachan, R.A., Topley, C.G. (Eds.), The Cadomian Orogeny.
1042 Geological Society Special Publication, pp. 81-94.
1043 Reymer, A., Schubert, G., 1984. Phanerozoic addition rates to the continental crust and
1044 crustal growth. Tectonics 3, 63-77.
1045 Roberts, N.M.W., Slagstad, T., Parrish, R.R., Norry, M.J., Marker, M., Horstwood,
1046 M.S.A., 2012. Sedimentary recycling in arc magmas: geochemical and U–Pb–Hf–O
1047 constraints on the Mesoproterozoic Suldal Arc, SW Norway. Contributions to
1048 Mineralogy and Petrology 165, 507-523.
1049 Roques, M., Pin, C., Duthou, J.-L., 1995. Prehercynian basement and Hercynian
1050 collision in the french Massif Central. Comptes Rendus de l'Académie des Sciences,
1051 Paris 320, 817-821.
1052 Rossi, P., Cocherie, A., Fanning, C.M., Deloule, É., 2006. Variscan to eo-Alpine events
1053 recorded in European lower-crust zircons sampled from the French Massif Central and
1054 Corsica, France. Lithos 87, 235-260.
1055 Rudnick, R.L., Fountain, D.M., 1995. Nature and composition of the continental crust: a
1056 lower crustal perspective. Reviews of Geophysics 33, 267-309.
1057 Rudnick, R.L., Gao, S., 2003. Composition of the continental crust, in: Rudnick, R.L.
1058 (Ed.), The Crust. Elsevier-Pergamon, Oxford, pp. 1-64.

1059 Samson, S.D., D'Lemos, R.S., 1998. U–Pb geochronology and Sm–Nd isotopic
1060 composition of Proterozoic gneisses, Channel Islands, UK. Journal of the Geological
1061 Society, London 155, 609-618.
1062 Samson, S.D., D'Lemos, R.S., Blichert-Toft, J., Vervoort, J., 2003. U–Pb
1063 geochronology and Hf–Nd isotope compositions of the oldest Neoproterozoic crust
1064 within the Cadomian orogen: new evidence for a unique juvenile terrane. Earth and
1065 Planetary Science Letters 208, 165-180.
1066 Sawyer, E.W., 2008. Atlas of Migmatites. NRC Research Press.
1067 Sircombe, K.N., Hazelton, M.L., 2004. Comparison of detrital zircon age distributions
1068 by kernel functional estimation. Sedimentary Geology 171, 91-111.
1069 Spencer, C.J., Kirkland, C.L., Taylor, R.J.M., 2016. Strategies towards statistically
1070 robust interpretations of in situ U–Pb zircon geochronology. Geoscience Frontiers 7,
1071 581-589.
1072 Stephan, T., Kroner, U.W.E., Romer, R.L., 2018. The pre-orogenic detrital zircon
1073 record of the Peri-Gondwanan crust. Geological Magazine, 1-27.
1074 Stern, R.A., Ali, K.A., Liégeois, J.P., Johnson, P.R., Kozdroj, W., Kattan, F.H., 2010.
1075 Distribution and significance of pre-Neoproterozoic zircons in juvenile Neoproterozoic
1076 igneous rocks of the Arabian Nubian Shield. American Journal of Science 310, 791-
1077 811.
1078 Stern, R.J., 2002. Crustal evolution in the East African Orogen: a neodymium isotopic
1079 perspective. Journal of African Earth Sciences 34, 109-117.
1080 Strachan, R.A., D'Lemos, R.S., Dallmeyer, R.D., 1996. Neoproterozoic evolution of an
1081 active plate margin: North Armorican Massif, France, in: Nance, R.D., Thompson, M.D.
1082 (Eds.), Avalonian and Related Peri-Gondwanan Terranes of the Circum–North Atlantic.
1083 Geological Society of America Special Paper, Boulder, Colorado, pp. 319-332.
1084 Talavera, C., Martínez Poyatos, D., González Lodeiro, F., 2015. SHRIMP U–Pb
1085 geochronological constraints on the timing of the intra-Alcudian (Cadomian) angular

1086 unconformity in the Central Iberian Zone (Iberian Massif, Spain). International Journal
1087 of Earth Sciences 104, 1739-1757.
1088 Talavera, C., Montero, P., Martínez Poyatos, D., Williams, I.S., 2012. Ediacaran to
1089 Lower Ordovician age for rocks ascribed to the Schist–Graywacke Complex (Iberian
1090 Massif, Spain): Evidence from detrital zircon SHRIMP U–Pb geochronology.
1091 Gondwana Research 22, 928-942.
1092 Taylor, S.R., McLennan, S.M., 1985. The Continental Crust: its Composition and
1093 Evolution. Blackwell, Oxford.
1094 Teixeira, R.J.S., Neiva, A.M.R., Silva, P.B., Gomes, M.E.P., Andersen, T., Ramos,
1095 J.M.F., 2011. Combined U–Pb geochronology and Lu–Hf isotope systematics by LAM–
1096 ICPMS of zircons from granites and metasedimentary rocks of Carrazeda de Ansiães
1097 and Sabugal areas, Portugal, to constrain granite sources. Lithos 125, 321-334.
1098 Thiéblemont, D., Guerrot, C., Simien, F., Zammit, C., 2017. Une compilation des âges
1099 radiochronologiques publiés antérieurement à 2016 sur le Massif armoricain. Inventaire
1100 et mise en forme des données, perspectives pour des acquisitions futures. Géologie de
1101 la France 1, 27-46.
1102 Toteu, S.F., Van Schmus, W.R., Penaye, J., Michard, A., 2001. New U–Pb and Sm–Nd
1103 data from north-central Cameroon and its bearing on the pre-Pan African history of
1104 central Africa. Precambrian Research 108, 45-73.
1105 Triantafyllou, A., Berger, J., Baele, J.-M., Diot, H., Ennih, N., Plissart, G., Monnier, C.,
1106 Watlet, A., Bruguier, O., Spagna, P., Vandycke, S., 2016. The Tachakoucht–Iriri–Tourtit
1107 arc complex (Moroccan Anti-Atlas): Neoproterozoic records of polyphased subduction-
1108 accretion dynamics during the Pan-African orogeny. Journal of Geodynamics 96, 81-
1109 103.
1110 Vermeesch, P., 2004. How many grains are needed for a provenance study? Earth and
1111 Planetary Science Letters 224, 441-451.

Vermeesch, P., 2012. On the visualisation of detrital age distributions. Chemical Geology 312-313, 190-194.

Vermeesch, P., 2013. Multi-sample comparison of detrital age distributions. Chemical Geology 341, 140-146.

Vermeesch, P., 2018. Dissimilarity measures in detrital geochronology. Earth-Science Reviews 178, 310-321.

Vermeesch, P., Resentini, A., Garzanti, E., 2016. An R package for statistical provenance analysis. Sedimentary Geology 336, 14-25.

Vervoort, J.D., Kemp, A.I.S., 2016. Clarifying the zircon Hf isotope record of crust–mantle evolution. Chemical Geology 425, 65-75.

Vervoort, J.D., Patchett, P.J., Blichert-Toft, J., Albarède, F., 1999. Relationships between Lu–Hf and Sm–Nd isotopic systems in the global sedimentary system. Earth and Planetary Science Letters 168, 79-99.

Vidal, P., 1980. L'évolution polyorogénique du Massif armoricain. Apport de la géochronologie et de la géochimie isotopique du strontium.

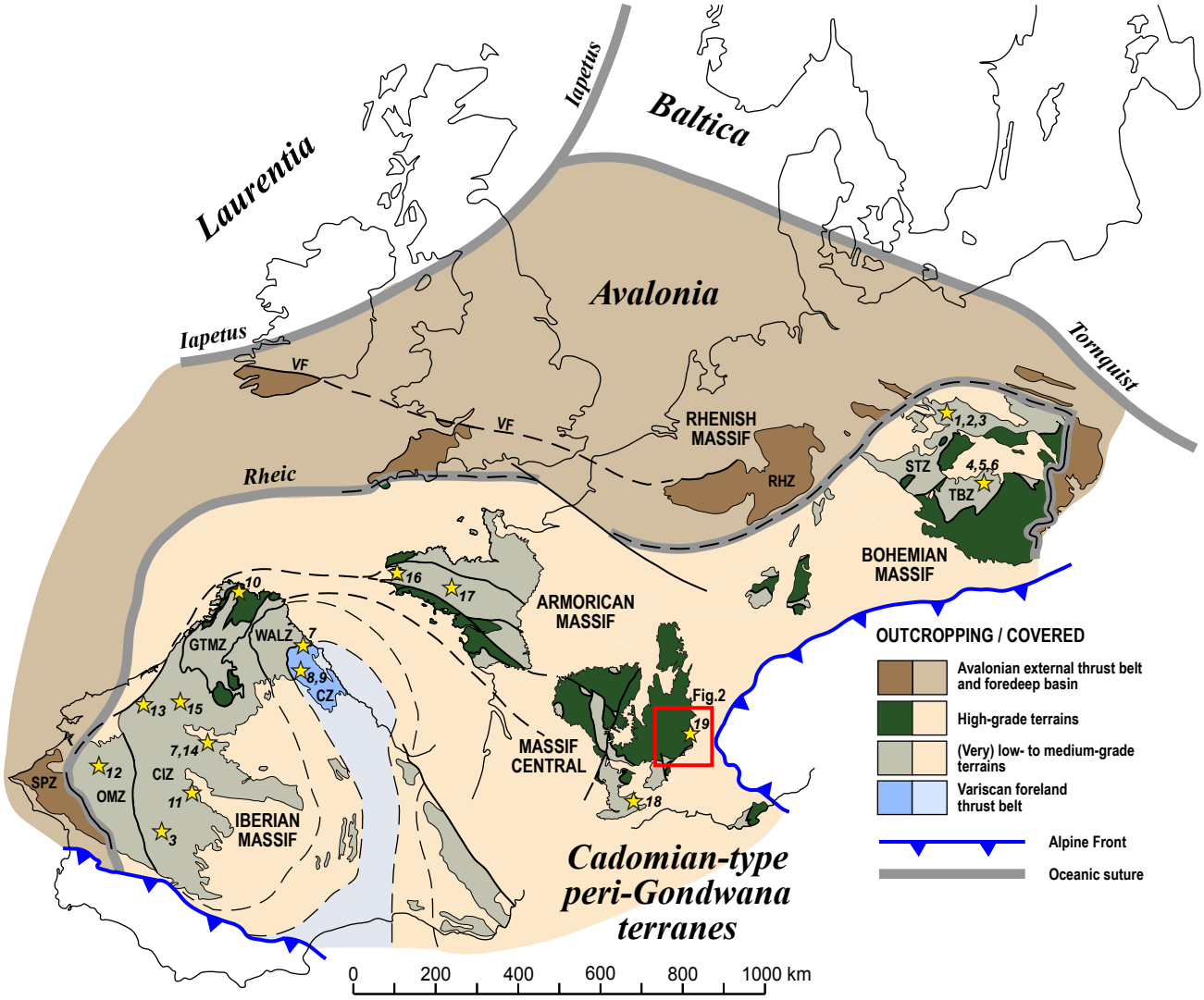
Villaros, A., Laurent, O., Couzinié, S., Moyen, J.F., Mintrone, M., 2018. Plutons and domes: the consequences of anatectic magma extraction—example from the southeastern French Massif Central. International Journal of Earth Sciences.

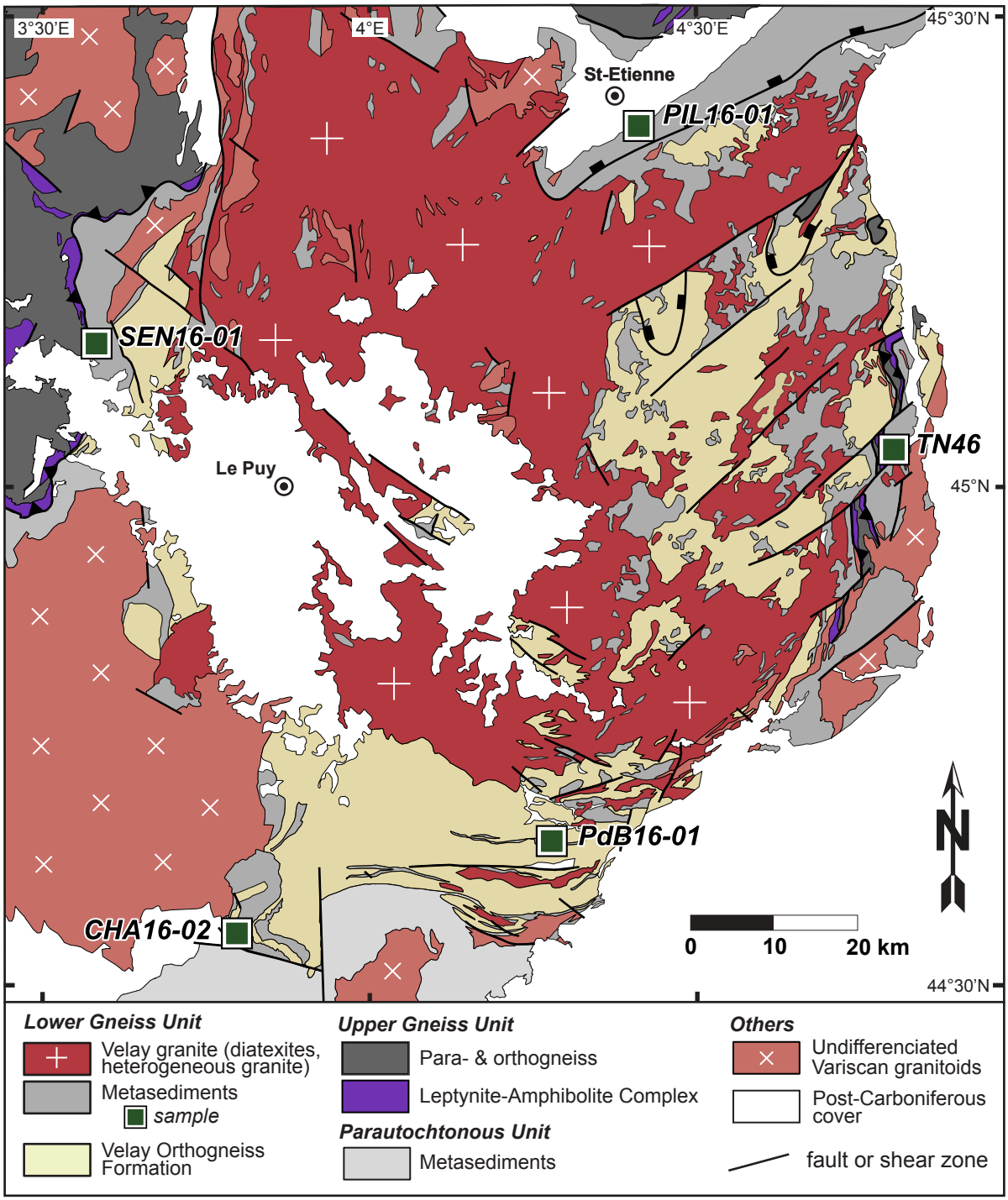
Wedepohl, K.H., 1995. The composition of the continental crust. Geochimica et Cosmochimica Acta 59, 1217-1232.

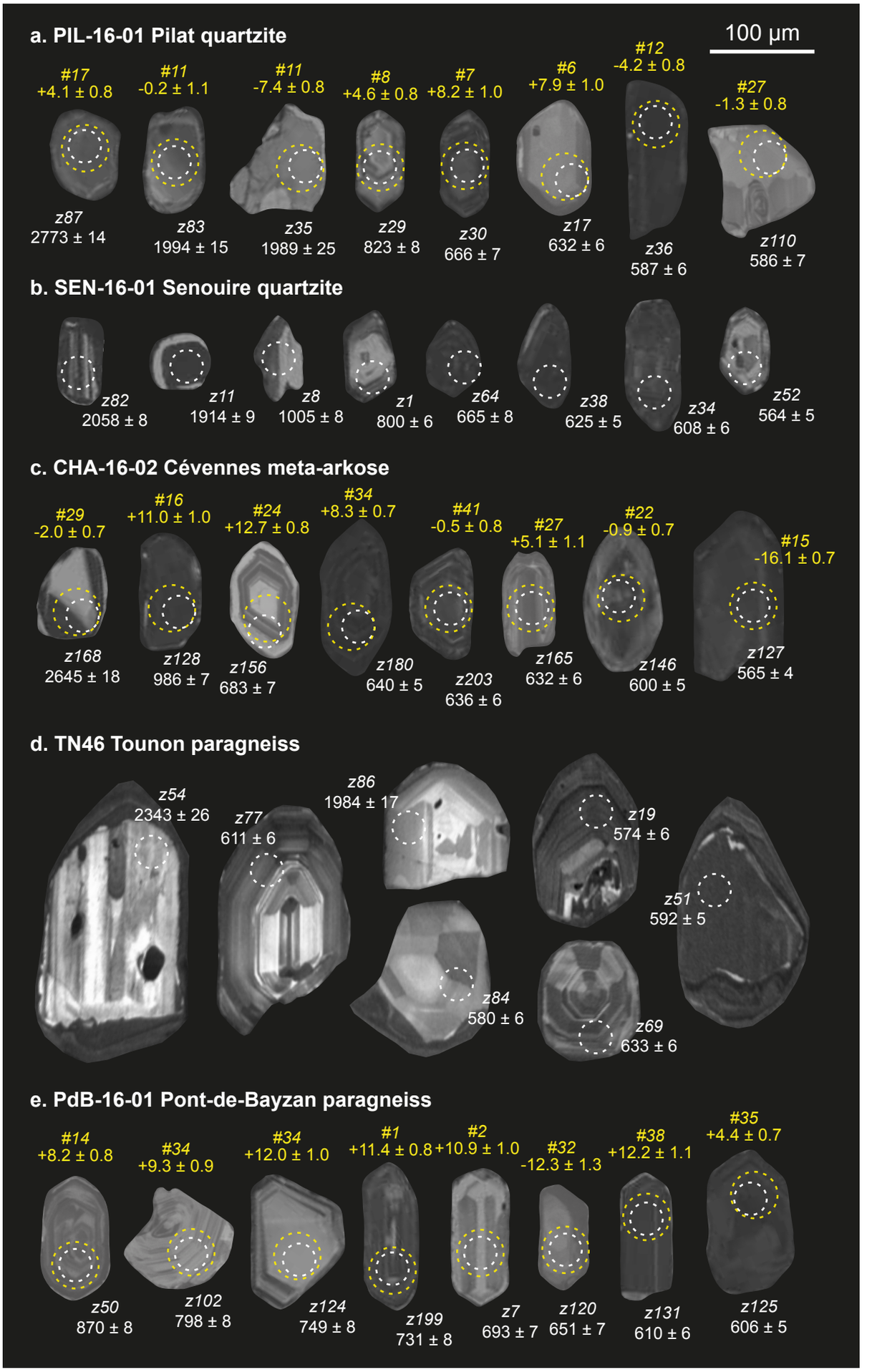
Žák, J., Sláma, J., 2017. How far did the Cadomian 'terranes' travel from Gondwana during early Palaeozoic? A critical reappraisal based on detrital zircon geochronology. International Geology Review, 1-20.

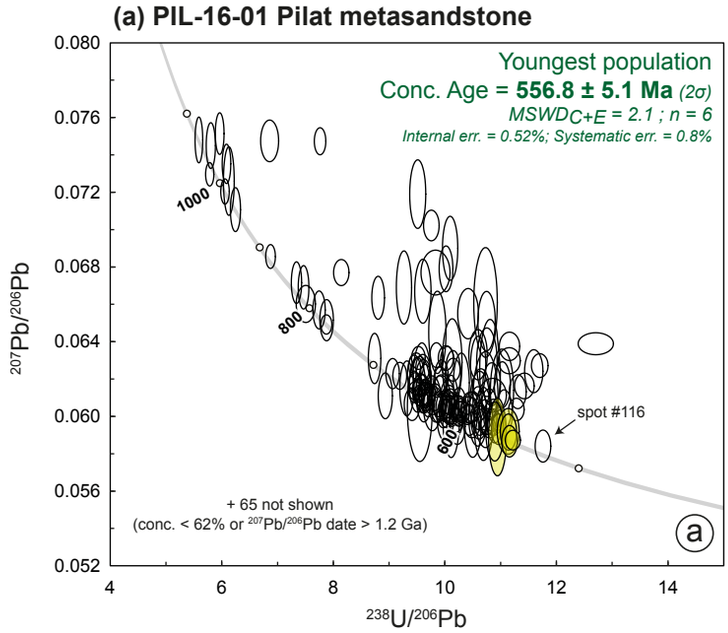
Zimmermann, U., Andersen, T., Madland, M.V., Larsen, I.S., 2015. The role of U-Pb ages of detrital zircons in sedimentology—An alarming case study for the impact of sampling for provenance interpretation. Sedimentary Geology 320, 38-50.

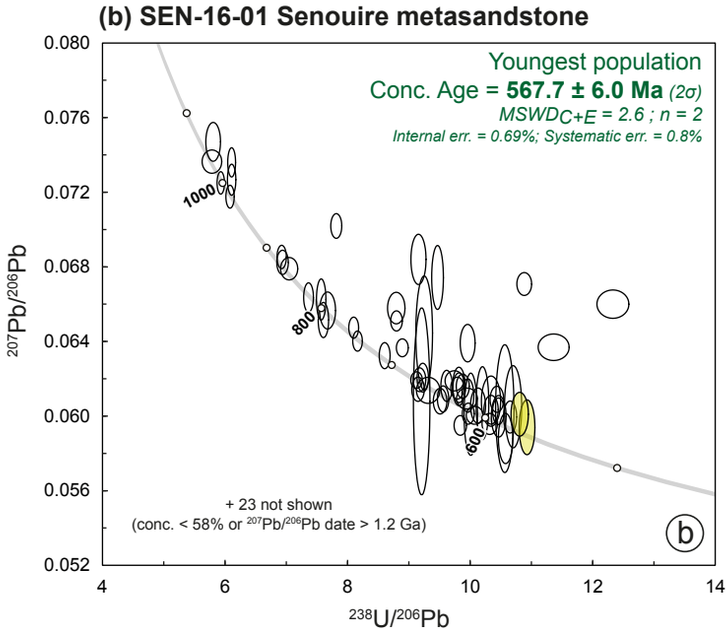
1138

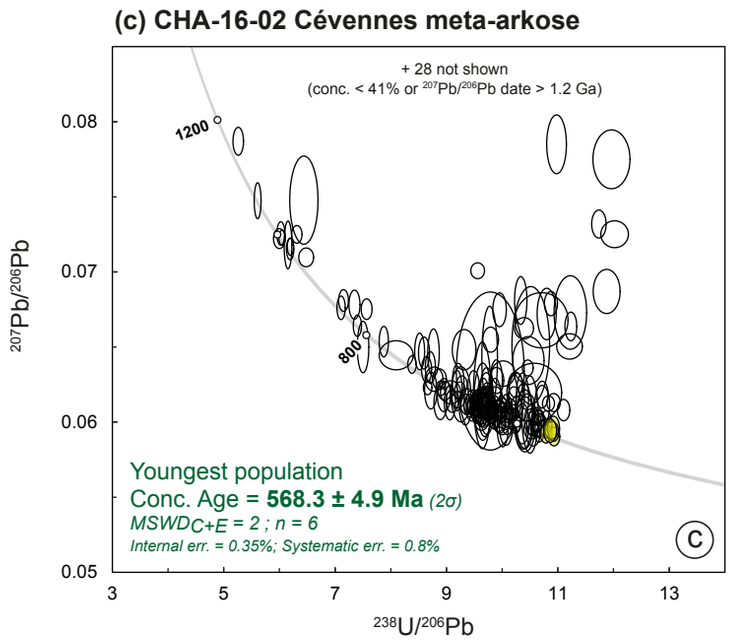

Laurentia
Iapetus
Baltica
Avalonia
Iapetus
Tornquist
Rheic
VF
VF
RHENISH MASSIF
RHZ
STZ
TBZ
1,2,3
4,5,6
BOHEMIAN MASSIF
ARMORICAN MASSIF
MASSIF CENTRAL
Fig.2
19
18
16
17
10
GTMZ
WALZ
7
8,9
CZ
13
15
7,14
12
SPZ
OMZ
CIZ
11
3
IBERIAN MASSIF
Cadomian-type peri-Gondwana terranes
0
200
400
600
800
1000 km
OUTCROPPING / COVERED
Avalonian external thrust belt and foredeep basin
High-grade terrains
(Very) low- to medium-grade terrains
Variscan foreland thrust belt
Alpine Front
Oceanic suture

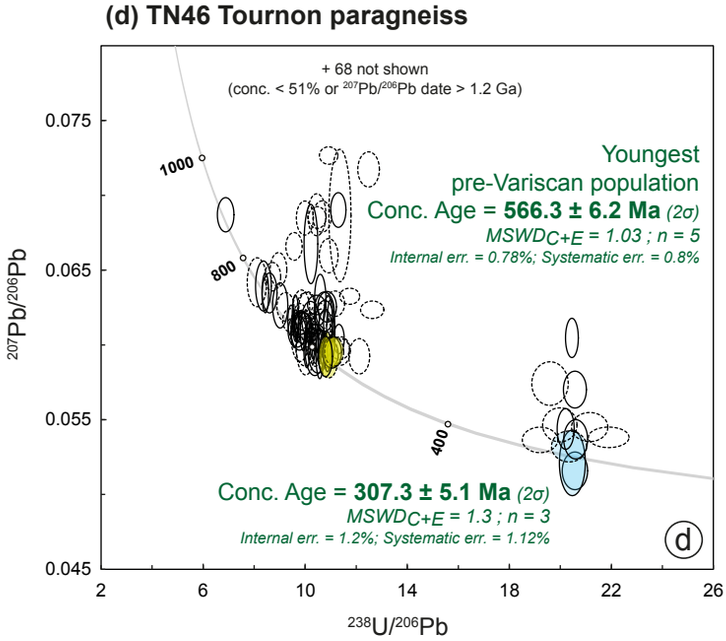

3°30'E
4°E
4°30'E
45°30'N
45°N
44°30'N
St-Etienne
PIL16-01
SEN16-01
Le Puy
TN46
PdB16-01
CHA16-02
N
0
10
20 km
Lower Gneiss Unit
Velay granite (diatexites, heterogeneous granite)
Metasediments
sample
Velay Orthogneiss Formation
Upper Gneiss Unit
Para- & orthogneiss
Leptynite-Amphibolite Complex
Parautochtonous Unit
Metasediments
Others
Undifferenciated Variscan granitoids
Post-Carboniferous cover
fault or shear zone

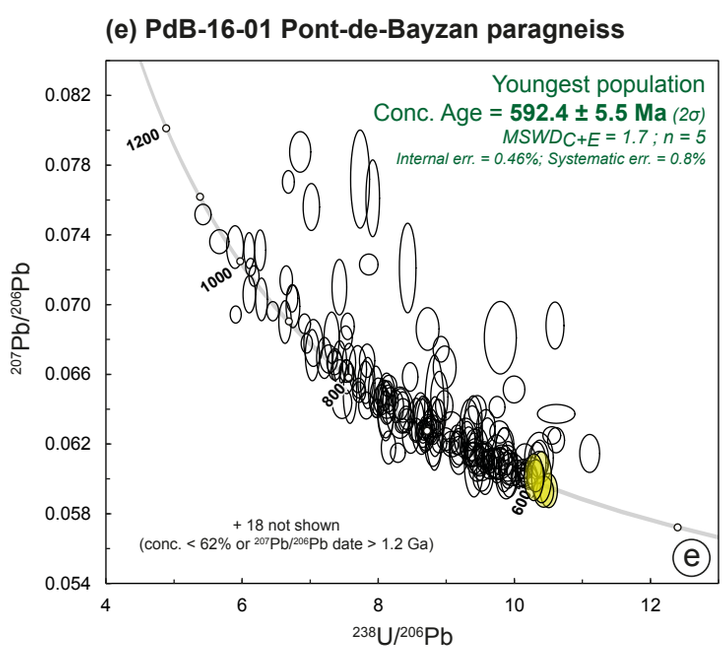

a. PIL-16-01 Pilat quartzite
100 µm
#17 +4.1 ± 0.8
#11 -0.2 ± 1.1
#11 -7.4 ± 0.8
#8 +4.6 ± 0.8
#7 +8.2 ± 1.0
#6 +7.9 ± 1.0
#12 -4.2 ± 0.8
#27 -1.3 ± 0.8
z87 2773 ± 14
z83 1994 ± 15
z35 1989 ± 25
z29 823 ± 8
z30 666 ± 7
z17 632 ± 6
z36 587 ± 6
z110 586 ± 7
b. SEN-16-01 Senouire quartzite
z82 2058 ± 8
z11 1914 ± 9
z8 1005 ± 8
z1 800 ± 6
z64 665 ± 8
z38 625 ± 5
z34 608 ± 6
z52 564 ± 5
c. CHA-16-02 Cévennes meta-arkose
#29 -2.0 ± 0.7
#16 +11.0 ± 1.0
#24 +12.7 ± 0.8
#34 +8.3 ± 0.7
#41 -0.5 ± 0.8
#27 +5.1 ± 1.1
#22 -0.9 ± 0.7
#15 -16.1 ± 0.7
z168 2645 ± 18
z128 986 ± 7
z156 683 ± 7
z180 640 ± 5
z203 636 ± 6
z165 632 ± 6
z146 600 ± 5
z127 565 ± 4
d. TN46 Tounon paragneiss
z54 2343 ± 26
z77 611 ± 6
z86 1984 ± 17
z19 574 ± 6
z51 592 ± 5
z84 580 ± 6
z69 633 ± 6
e. PdB-16-01 Pont-de-Bayzan paragneiss
#14 +8.2 ± 0.8
#34 +9.3 ± 0.9
#34 +12.0 ± 1.0
#1 +11.4 ± 0.8
#2 +10.9 ± 1.0
#32 -12.3 ± 1.3
#38 +12.2 ± 1.1
#35 +4.4 ± 0.7
z50 870 ± 8
z102 798 ± 8
z124 749 ± 8
z199 731 ± 8
z7 693 ± 7
z120 651 ± 7
z131 610 ± 6
z125 606 ± 5

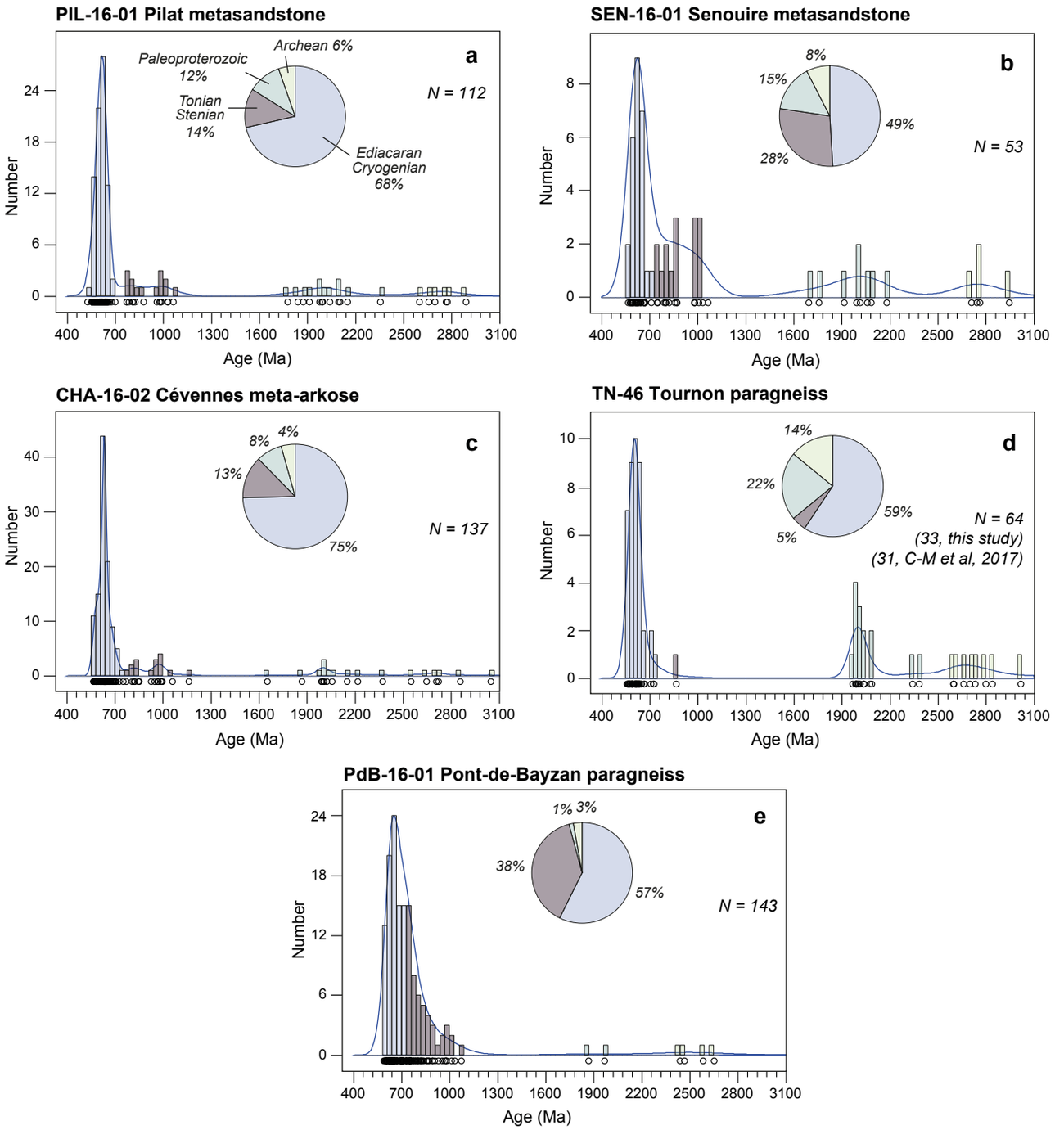

(a) PIL-16-01 Pilat metasandstone
Youngest population
Conc. Age = 556.8 ± 5.1 Ma (2σ)
MSWDC+E = 2.1 ; n = 6
Internal err. = 0.52%; Systematic err. = 0.8%
spot #116
+ 65 not shown
(conc. < 62% or 207Pb/206Pb date > 1.2 Ga)
a
207Pb/206Pb
238U/206Pb

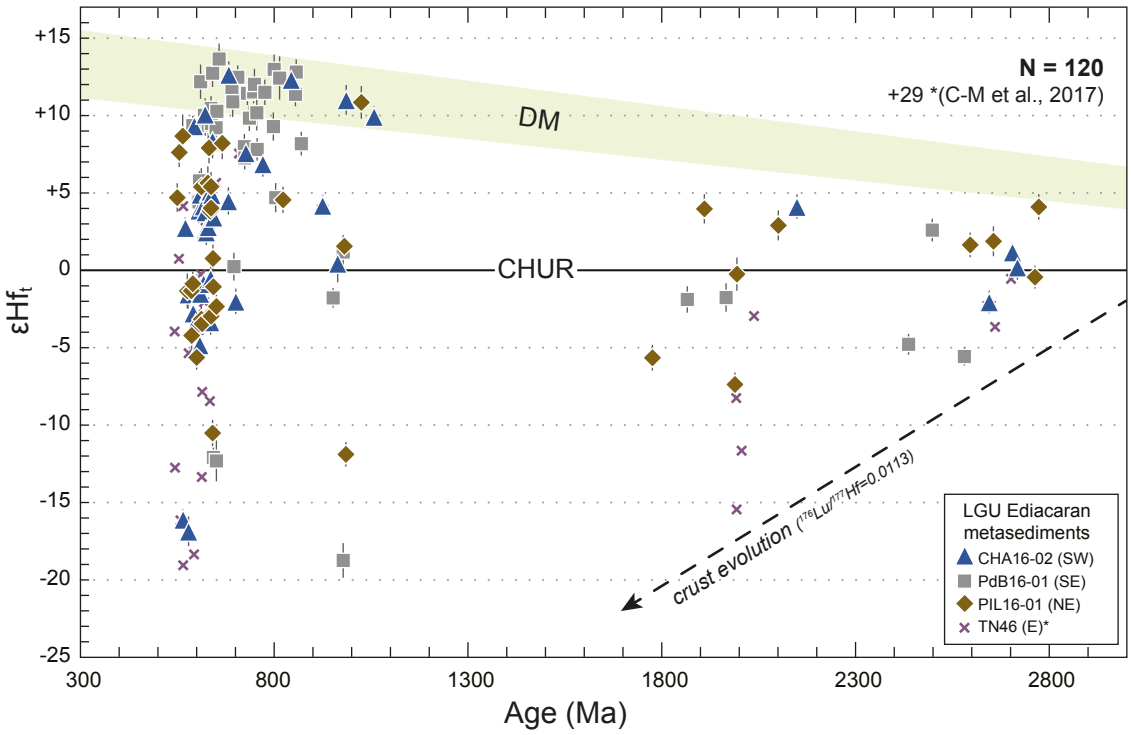

(b) SEN-16-01 Senouire metasandstone
Youngest population
Conc. Age = 567.7 ± 6.0 Ma (2σ)
MSWDC+E = 2.6 ; n = 2
Internal err. = 0.69%; Systematic err. = 0.8%
+ 23 not shown
(conc. < 58% or 207Pb/206Pb date > 1.2 Ga)
b
207Pb/206Pb
238U/206Pb

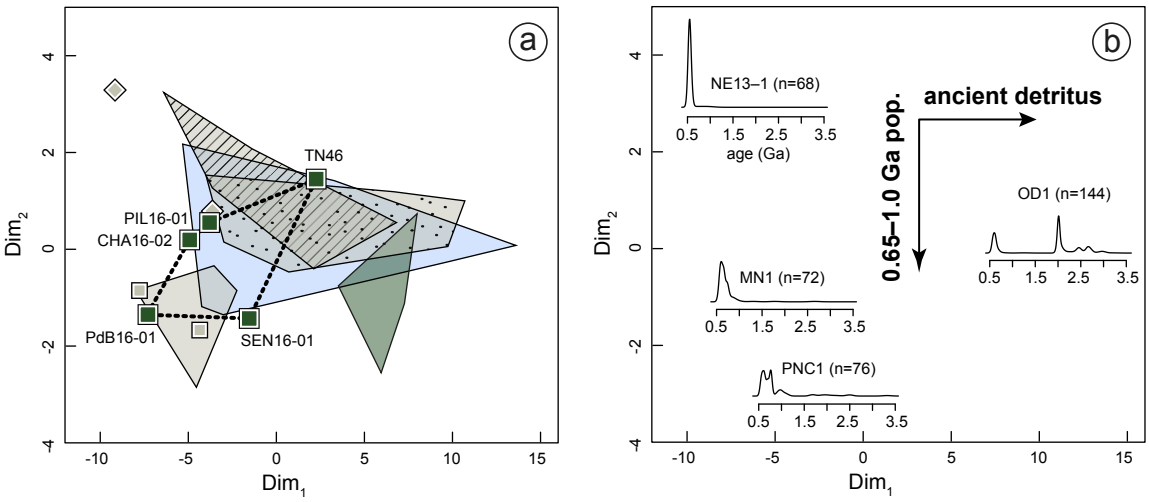

(c) CHA-16-02 Cévennes meta-arkose
+ 28 not shown
(conc. < 41% or 207Pb/206Pb date > 1.2 Ga)
Youngest population
Conc. Age = 568.3 ± 4.9 Ma (2σ)
MSWDC+E = 2 ; n = 6
Internal err. = 0.35%; Systematic err. = 0.8%
c
207Pb/206Pb
238U/206Pb


(d) TN46 Tournon paragneiss
+ 68 not shown
(conc. < 51% or 207Pb/206Pb date > 1.2 Ga)
Youngest
pre-Variscan population
Conc. Age = 566.3 ± 6.2 Ma (2σ)
MSWDC+E = 1.03 ; n = 5
Internal err. = 0.78%; Systematic err. = 0.8%
Conc. Age = 307.3 ± 5.1 Ma (2σ)
MSWDC+E = 1.3 ; n = 3
Internal err. = 1.2%; Systematic err. = 1.12%
d
207Pb/206Pb
238U/206Pb


(e) PdB-16-01 Pont-de-Bayzan paragneiss
Youngest population
Conc. Age = 592.4 ± 5.5 Ma (2σ)
MSWDC+E = 1.7 ; n = 5
Internal err. = 0.46%; Systematic err. = 0.8%
+ 18 not shown
(conc. < 62% or 207Pb/206Pb date > 1.2 Ga)
e
207Pb/206Pb
238U/206Pb


PIL-16-01 Pilat metasandstone
a
N = 112
Archean 6%
Paleoproterozoic 12%
Tonian Stenian 14%
Ediacaran Cryogenian 68%
Number
Age (Ma)
SEN-16-01 Senouire metasandstone
b
N = 53
8%
15%
49%
28%
Number
Age (Ma)
CHA-16-02 Cévennes meta-arkose
c
N = 137
4%
8%
13%
75%
Number
Age (Ma)
TN-46 Tournon paragneiss
d
N = 64
(33, this study)
(31, C-M et al, 2017)
14%
22%
59%
5%
Number
Age (Ma)
PdB-16-01 Pont-de-Bayzan paragneiss
e
N = 143
1%
3%
38%
57%
Number
Age (Ma)


N = 120
+29 *(C-M et al., 2017)
DM
CHUR
crust evolution (176Lu/177Hf=0.0113)
LGU Ediacaran metasediments
CHA16-02 (SW)
PdB16-01 (SE)
PIL16-01 (NE)
TN46 (E)*
εHft
Age (Ma)
+15
+10
+5
0
-5
-10
-15
-20
-25
300
800
1300
1800
2300
2800



High-grade metasediments

Galicia–Trás-os-Montes (n=5)

Lower Gneiss Unit (Eastern Massif Central)

(Very) Low- to medium-grade (meta)sediments

Central Iberian/West Asturian–Leonese (n=10, 1 excluded)

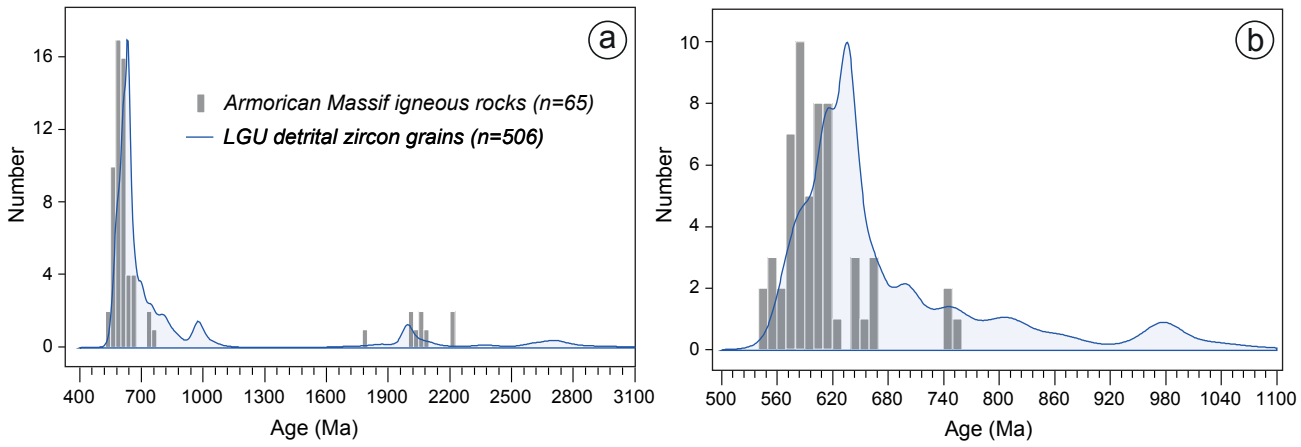
Saxo-Thuringian (n=16)

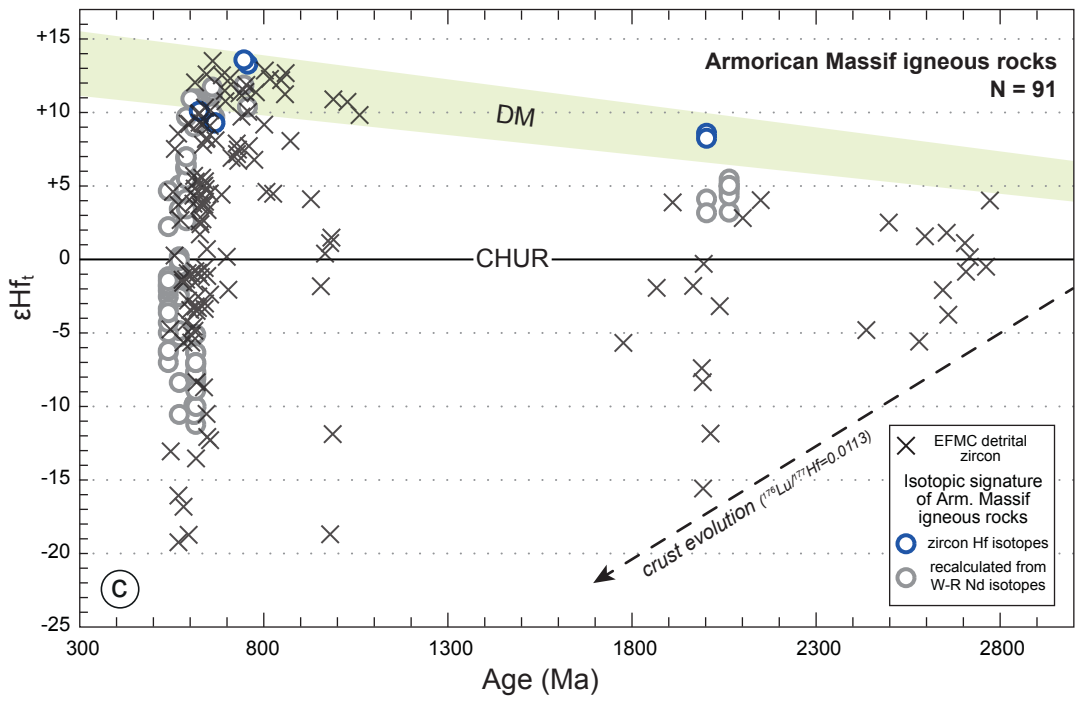
Teplá-Barrandian (n=6)

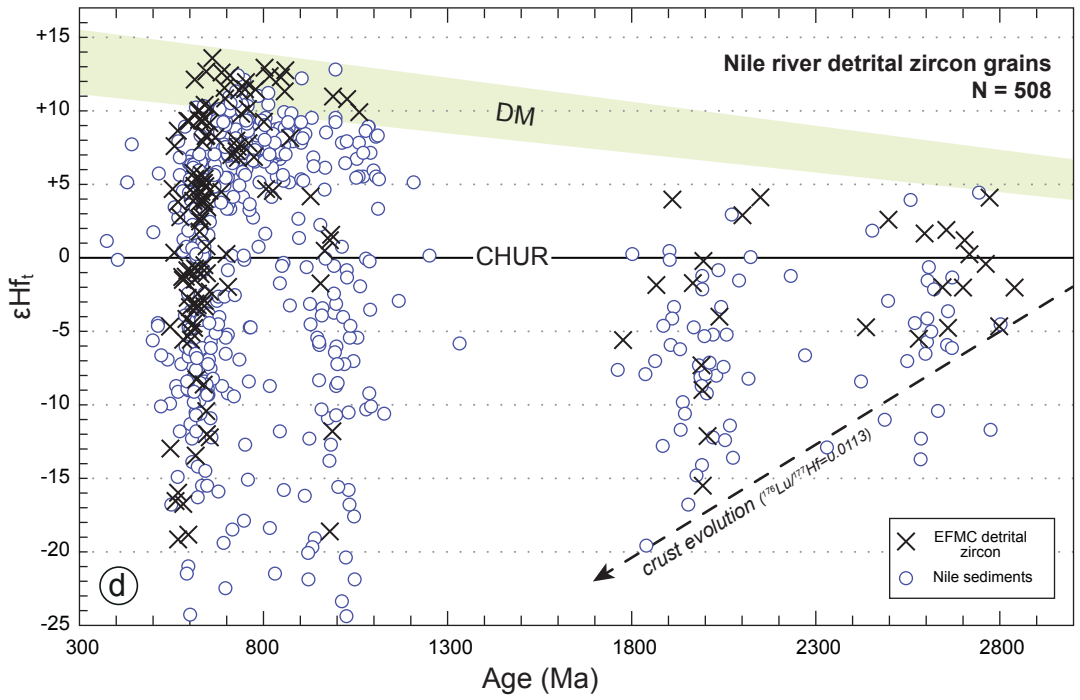
Cantabrian (n=6)

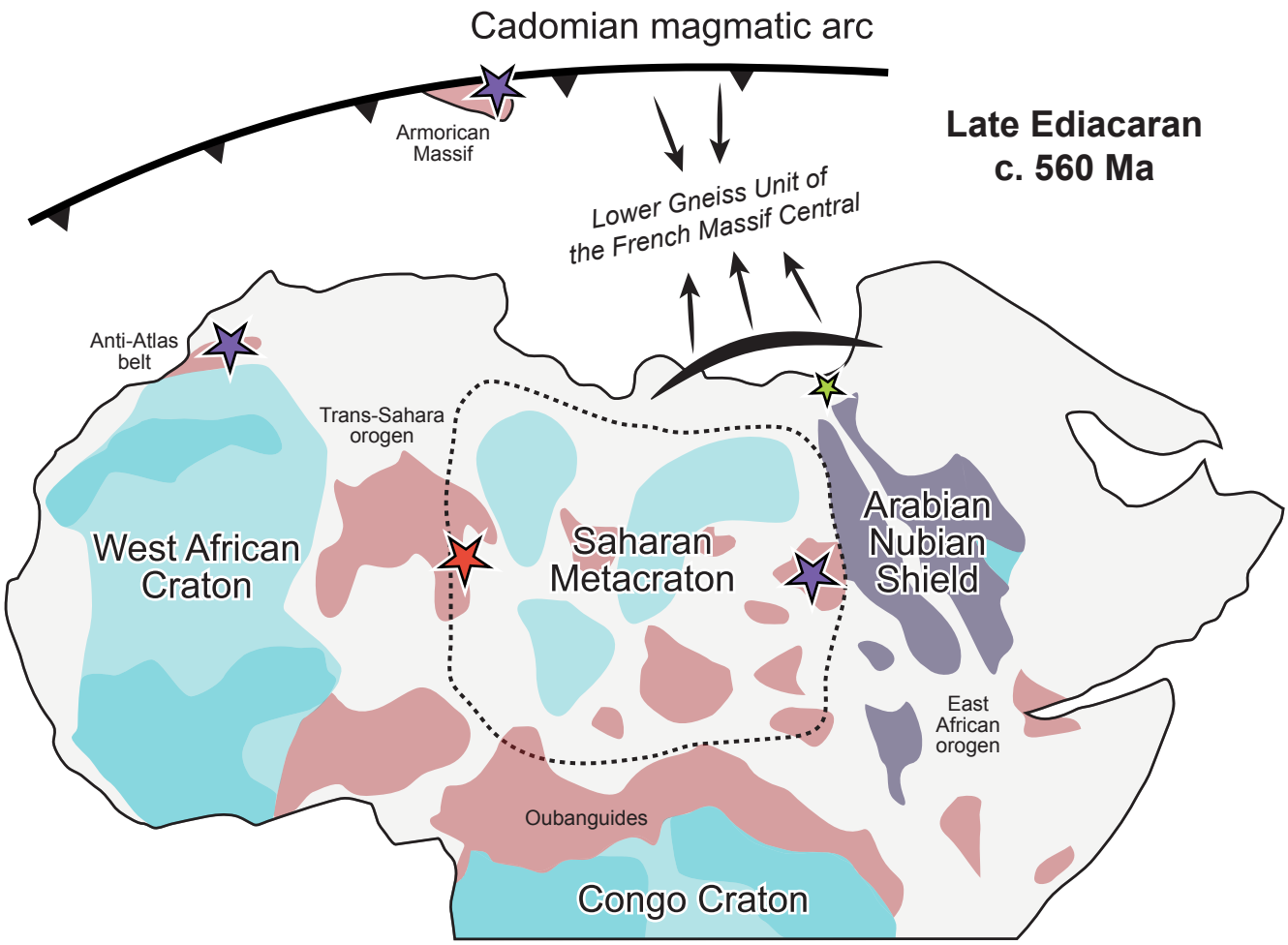
Montagne Noire (Southern Massif Central)

Armorican Massif


a
Armorican Massif igneous rocks (n=65)
LGU detrital zircon grains (n=506)
Number
Age (Ma)
b
Number
Age (Ma)

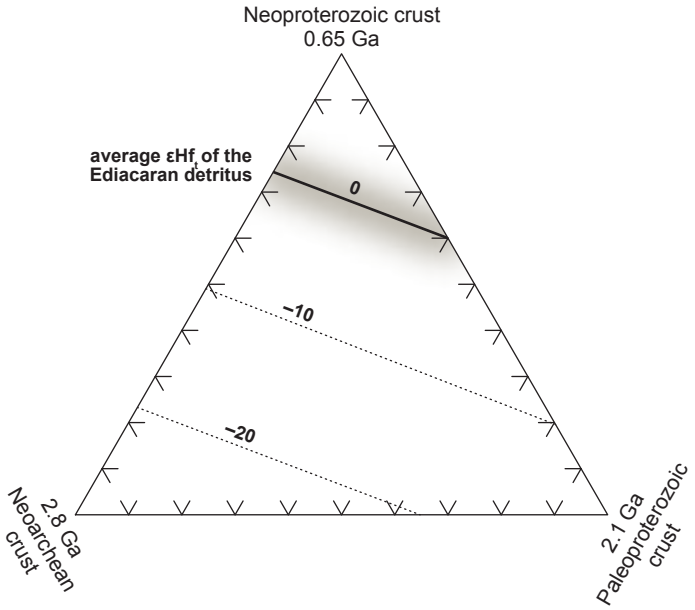

Armorican Massif igneous rocks
N = 91
DM
CHUR
εHf$_t$
crust evolution ($^{176}Lu/^{177}Hf$=0.0113)
EFMC detrital zircon
Isotopic signature of Arm. Massif igneous rocks
zircon Hf isotopes
recalculated from W-R Nd isotopes
c
Age (Ma)


Nile river detrital zircon grains
N = 508
DM
CHUR
εHf$_t$
crust evolution ($^{176}Lu/^{177}Hf$=0.0113)
EFMC detrital zircon
Nile sediments
d
Age (Ma)



Panafrican orogens

- Ediacaran – late Cryogenian crust with supra to subchondritic Nd-Hf signatures
- Ediacaran – late Tonian crust with strictly suprachondritic Nd-Hf signatures
- early Cryogenian – Tonian crust with suprachondritic Nd signatures
- early Cryogenian – Tonian crust with subchondritic Nd signatures
- Stenian crust
- Paleoproterozoic to Archean crust (exposed/covered craton)


Neoproterozoic crust
0.65 Ga
average εHf$_t$ of the
Ediacaran detritus
0
−10
−20
2.8 Ga
Neoarchean
crust
2.1 Ga
Paleoproterozoic
crust